SIAM J. MATH. ANAL.
Vol. 51, No. 1, pp. 276–320

A GINZBURG–LANDAU-TYPE PROBLEM FOR HIGHLY ANISOTROPIC NEMATIC LIQUID CRYSTALS*

DMITRY GOLOVATY†, PETER STERNBERG‡, AND RAGHAVENDRA VENKATRAMAN‡

Abstract. We carry out an asymptotic analysis of a variational problem relevant in the studies of nematic liquid crystalline films when one elastic constant dominates over the others, namely, $\inf E_\varepsilon(u)$, where $E_\varepsilon(u) := \frac{1}{2}\int_\Omega \left\{\varepsilon\,|\nabla u|^2 + \frac{1}{\varepsilon}\,(|u|^2-1)^2 + L\,(\operatorname{div} u)^2\right\} dx$. Here $u : \Omega \to \mathbb{R}^2$ is a vector field, $0 < \varepsilon \ll 1$ is a small parameter, and $L > 0$ is a fixed constant, independent of ε. We identify a candidate for the Γ-limit E_0, which is a sum of a bulk term penalizing divergence and an Aviles–Giga-type wall energy involving the cube of the jump in the tangential component of the $\mathbb{S}^1$-valued nematic director. We establish the lower bound and provide the recovery sequence for this candidate within a restricted class. Then we consider a set of variational problems for E_0 arising from various choices of domain geometry and boundary conditions. We demonstrate that the criticality conditions for E_0 can be expressed as a pair of scalar conservation laws that share characteristics. We use the method of characteristics to analytically construct critical points of E_0 that we observe numerically.

Key words. nematic liquid crystals, Oseen–Frank energy, Aviles–Giga energy, conservation laws, Γ-convergence

AMS subject classifications. 35Q56, 35L65, 49K20

DOI. 10.1137/18M1178360

1. Introduction.

Describing the elastic energy in nematic liquid crystal models involves making a choice of the elastic constants appearing as coefficients in front of the various terms penalizing spatial variations. Whether in director theories such as Oseen–Frank, where the unknown is a unit vector $n \in \mathbb{R}^2$ or $\mathbb{R}^3$, or within the Landau–de Gennes Q-tensor model where Q is a symmetric, traceless 3×3 matrix [23, 26], some studies pursue an isotropic, or equal constants, choice where the elastic energy density is given simply by $|\nabla n|^2$ or $|\nabla Q|^2$. Others opt for more generality and consider, for instance, three distinct coefficients multiplying the square of the divergence and the squares of the components of the curl along and perpendicular to the director, respectively. However, in response to numerous studies by materials scientists who suggest that interesting morphologies in liquid crystals are related to disparities in the values of the elastic constants [10, 27], here we consider a model variational problem with extreme disparity in elastic constants and explore the implications of this choice of elastic coefficients on the structure of minimizers.

We will focus our study on a problem in two dimensions with a thin nematic film in mind, and so for a bounded, Lipschitz domain $\Omega \subset \mathbb{R}^2$ we consider the following variational problem:

$$\inf E_\varepsilon(u), \quad \text{where} \quad E_\varepsilon(u) := \frac{1}{2}\int_\Omega \left\{\varepsilon\,|\nabla u|^2 + \frac{1}{\varepsilon}\,(|u|^2-1)^2 + L\,(\operatorname{div} u)^2\right\} dx. \tag{1.1}$$

*Received by the editors April 2, 2018; accepted for publication (in revised form) November 29, 2018; published electronically February 7, 2019.
http://www.siam.org/journals/sima/51-1/M117836.html
Funding: The work of the first author was supported by National Science Foundation grant DMS-1729538. The work of the second and third authors was supported by National Science Foundation grants DMS-1101290 and DMS-1362879. The work of the third author was also supported by an Indiana University College of Arts and Sciences Dissertation Year Fellowship.

†Department of Mathematics, University of Akron, Akron, OH 44325 (dgolovaty@gmail.com).
‡Department of Mathematics, Indiana University, Bloomington, IN 47405 (sternber@indiana.edu, rvenkatr@umail.iu.edu).

Here $u : \Omega \to \mathbb{R}^2$ is a vector field, $0 < \varepsilon \ll 1$ is a small parameter, and $L > 0$ is a fixed constant, independent of ε. In general, we will augment (1.1) with Dirichlet boundary conditions $u = g$ on $\partial\Omega$ for given $g : \partial\Omega \to \mathbb{S}^1$. We point out that in light of the two-dimensional identity

$$(\operatorname{div} u)^2 + |\operatorname{curl} u|^2 = |\nabla u|^2 + \text{ null Lagrangian}$$

it suffices in this study to just penalize the divergence and not to include the curl as well. As u is not a unit vector, (1.1) is not a director model per se but rather bears more resemblance to the Ericksen model with variable degree of orientation [13]. Still it maintains some essential features of both the Oseen–Frank and Landau–de Gennes models that we wish to focus on in this investigation.

In order to orient the reader as to how this energy compares with other more familiar models, we point out that when the positive parameter L is dropped, one is left with precisely the simplified Ginzburg–Landau model

$$\text{(BBH)} \qquad \frac{1}{2}\int_\Omega \left\{ \varepsilon\,|\nabla u|^2 + \frac{1}{\varepsilon}\,(|u|^2 - 1)^2 \right\} dx$$

thoroughly examined in [7] under the scaling $\frac{1}{\varepsilon}E_\varepsilon$. For $\varepsilon \ll 1$, minimizers u_ε of that problem are characterized by so-called Ginzburg–Landau vortices with $u_\varepsilon \approx f_\varepsilon(r)\big(\cos\theta, \pm\sin\theta\big)$ near a zero that carries degree ± 1. On the other hand, formally passing to the limit $L \to \infty$ in (1.1), one is led to a divergence-free constraint, in which case, at least for simply connected domains Ω, one can introduce a stream function ψ via $\nabla^\perp \psi = u$. Then E_ε transforms into

$$\text{(AG)} \qquad \frac{1}{2}\int_\Omega \left\{ \varepsilon |D^2\psi|^2 + \frac{1}{\varepsilon}(|\nabla\psi|^2 - 1)^2 \right\} dx,$$

which is precisely the well-studied Aviles–Giga model; see, e.g., [5, 4, 8, 9, 17, 19, 22] and the references therein. Singular structures for that model emerging in the $\varepsilon \to 0$ limit take the form of domain walls—generically, curves—across which the normal component of $\nabla\psi$ jumps. Though we do not pursue it in this article, an interesting direction would be to make a rigorous study of the limit $L \to \infty$ in relating our problem to (AG). We should also mention that there are a multitude of models bearing some resemblance to E_ε coming from the micromagnetics community, including, for instance, the ones studied in [17, 3, 18, 24] where the L^2-norm of the divergence is replaced by an H^{-1}-norm, which is then considered with a different scaling.

From this perspective then, our problem rests between the two models (BBH) and (AG), and indeed we will find a rich array of singular structures playing a role, including Ginzburg–Landau-type vortices, which in the scaling of (1.1) are relatively expensive; domain walls which end up contributing $O(1)$ to the energy E_ε; and divergence-free vortices of the form $f_\varepsilon(r)\,\widehat{e}_\theta$, where $\widehat{e}_\theta := \big(-\sin\theta, \cos\theta\big)$, whose asymptotic contribution to the energy is zero.

A natural goal is to identify a candidate for the Γ-limit of the sequence $\{E_\varepsilon\}$ as $\varepsilon \to 0$, and with this in mind, a first issue is to determine the appropriate space of competitors for such a limit and to explore what kind of compactness properties hold for sequences of $H^1(\Omega;\mathbb{R}^2)$ functions, say $\{w_\varepsilon\}$, satisfying a uniform energy bound $E_\varepsilon(w_\varepsilon) < C$. One is naturally led to consider the Hilbert space $H_{\text{div}}\,(\Omega;\mathbb{R}^2)$ consisting of L^2 vector fields having L^2-divergence, and it is immediate that $\{w_\varepsilon\}$ will be weakly compact in this space, with an $\mathbb{S}^1$-valued limit. Such mappings can, in general, have

tangential components that jump across curves, though their normal components cannot jump. In Theorem 3.1 we note that through a minor modification of the compactness result of [12] one may also show strong convergence, up to subsequences, in $L^p(\Omega;\mathbb{R}^2)$ for any $p<\infty$; see also [4] for an independent proof of compactness in the Aviles–Giga setting.

From the standpoint of constructing energy-efficient sequences, and ultimately recovery sequences for Γ-convergence, the resolution of a jump in the tangential components of an $\mathbb{S}^1$-valued map, say w, across a wall leads one to consider a Modica–Mortola type of heteroclinic connection linking the tangential values $\pm\sqrt{1-(w\cdot\nu)^2}$ across an interface having normal ν. With these heuristics in mind, and denoting the one-sided traces along such a jump set J_u by u_+ and u_-, one is led to a candidate for the Γ-limit of the form

$$E_0(u) := \frac{L}{2}\int_\Omega (\operatorname{div} u)^2\,dx + \frac{1}{6}\int_{J_u\cap\Omega} |u_- - u_+|^3\,d\mathcal{H}^1 + \frac{1}{6}\int_{\partial\Omega} |u_{\partial\Omega} - g|^3\,d\mathcal{H}^1. \tag{1.2}$$

We note that the cubic dependence on the jump across J_u is identical to that found in the asymptotics for (AG). However, we also point out the presence of the boundary integral in (1.2) measuring possible jumps in the tangential component along $\partial\Omega$, a feature of our model not typically found in the Aviles–Giga problem.

The form of E_0 suggests that the space of definition for the Γ-limit must be a subset of those vector fields in $H_{\mathrm{div}}(\Omega;\mathbb{S}^1)$ having a rectifiable jump set with the cube of the jump in the one-sided traces being integrable. The difficulty lies in the fact that energy-bounded sequences may not have limits lying in the space of functions of bounded variation, an effect first elucidated for (AG) in [4], so identification of a natural space is nontrivial. In [4, 9] the authors identify what would appear to be the right space for establishing Γ-convergence for the Aviles–Giga functional, introducing the notion of "entropy measures," but to date the construction of a recovery sequence remains an open problem for (AG). We do not pursue here the interesting question of whether some analogue of the results in [9] on the structure of elements of this new space holds for the energy E_ε in (1.1).

Instead we will present arguments for the Γ-limit lower bound and for the recovery sequence under the *assumption* of the limit lying in $H_{\mathrm{div}}(\Omega;\mathbb{S}^1)\cap BV(\Omega;S^1)$. This is the content of Theorem 3.2. We note that similar difficulties arise when partial Γ-convergence results are obtained in micromagnetic models such as [3]. Our technique for proving lower-semicontinuity adapts the Jin–Kohn entropy [19] and is based upon the corresponding result from [5]. For the recovery sequence we adopt the rather ingenious and nontrivial construction of Conti and De Lellis for (AG) (cf. [8]), with care taken to verify that the divergence term in E_ε—not present in (AG)—does not contribute to the energy in a neighborhood of the jump set.

After presenting the arguments for Γ-convergence within this special class, we turn to the analysis of the behavior of minimizers of the presumed Γ-limit E_0 in various geometries and under various boundary conditions g. That is, we want to focus on the question of what kinds of morphologies one should expect to see for very disparate elastic constants, and in the process we will develop new tools for carrying out such an investigation.

We begin this pursuit by establishing various notions of criticality for E_0. In Theorem 4.1 we show that in the bulk, that is, away from the jump set J_u, criticality of a vector field u implies that the gradient of divergence lies in the direction of u. When u is locally lifted to $u=e^{i\theta}$, this leads to a pair of conservation laws for the phase θ and the divergence of u, both sharing the same characteristics; cf. Corollary 4.2.

This makes for an interesting comparison with the presumed Γ-limit of (AG), where, for example, the authors of [12] exploit the presence of a single conservation law for θ writing $\nabla^\perp u = e^{i\theta}$, where u solves the eikonal equation. We also derive in (4.2) and (4.3) a natural boundary condition holding along J_u relating the normal component of u to the jump in the divergence across the wall, and in (4.3) a criticality condition yielding stationarity of the wall itself that not surprisingly involves its curvature. We use these conditions in the rest of the paper to build critical points for specific examples.

In section 5 we specialize our study of minimizers of E_0 to the case where Ω is either a disc or an annulus. Depending on the choice of the $\mathbb{S}^1$-valued boundary condition g, we find that minimizers may or may not develop walls and tend to follow $\widehat{e}_\theta$ as much as possible. In particular, for "hedgehog" boundary conditions $g(\theta) = \widehat{e}_r := (\cos\theta, \sin\theta)$ in the disc, we can establish an explicit formula for the minimizer as a vector field that behaves like $\widehat{e}_\theta$ near the origin and then unwinds to $\widehat{e}_r$ to accommodate the boundary conditions; cf. Theorem 5.1. This result is reminiscent of a similar observation made in [16] for the three-dimensional Oseen–Frank model in a ball with hedgehog boundary conditions when divergence is penalized heavily. Perhaps the most interesting case to us is for the disc under the choice $g(\theta) = (\cos\theta, -\sin\theta)$. Here our numerics reveal a rather dramatic dependence of the wall geometry and location on the value of the parameter L, and through the three criticality conditions and system of conservation laws derived in section 4 we are able to build a critical point that appears to capture this complicated morphology, at least in a particular parameter regime. We conclude this section with an example posed in an annulus where our analysis suggests that in some parameter regime, a minimizer prefers to have a wall that coincides with the boundary.

Finally, in section 6 we pose the problem of minimizing E_0 in a rectangle subject to constant Dirichlet data on the top and bottom of the form $(\pm\sqrt{1-a^2}, a)$ for $a \in [0,1)$ and periodic boundary conditions on the sides. What motivates our choice of periodic boundary conditions is the wish to understand under what conditions the transition from the top to the bottom involves a one-dimensional wall construction as opposed to a more complicated two-dimensional cross-tie-type scenario as appears in various micromagnetic studies such as [3, 11]. This question was raised and partially addressed for the case of anisotropic elastic energy—though not "extreme anisotropic" elastic energy in the sense of our present work—in the articles [6, 14].

Our focus at the beginning of this section is to revisit the question of compactness and Γ-convergence within the one-dimensional context where competitors only vary with y. In Theorem 6.1 we show that energy bounded sequences do necessarily have subsequential limits whose third power lies in $BV(-H, H)$, where $2H$ is the height of the rectangle. We then state the Γ-convergence result in one dimension; cf. Theorem 6.2.

After then giving a complete characterization of one-dimensional minimizers in Theorem 6.4 we conclude with a two-dimensional construction of a critical point with cross-ties, again utilizing the criticality conditions and conservation laws. The energy of this critical point is then compared to the minimal one-dimensional energy to reveal in Theorem 6.6 that there exists a finite interval (L_0, L_1) of L-values—bounded away from zero—for which the one-dimensional minimizers from Theorem 6.4 do *not* minimize the full two-dimensional E_0 energy. Here we use a combination of analysis and simple numerical integration to demonstrate that the E_0 energy of our critical point with cross-ties is below the energy of one-dimensional minimizers when $L \in (L_0, L_1)$. Additional numerical simulations of the gradient flow for the energy E_ε show

that the (local) minimizers of E_ε have morphology and energy similar to our cross-tie construction within the interval of L-values where the energy of this construction is lower than that of the one-dimensional minimizers. In fact, these simulations also suggest that a different cross-tie-type structure develops as L is increased further, and this structure has energy that is still lower than that of the one-dimensional critical point.

We begin our article with a section introducing notation and recalling key notions regarding the function spaces $H_{\mathrm{div}}(\Omega;\mathbb{R}^2)$ and $BV(\Omega;\mathbb{R}^2)$.

2. Preliminaries. Throughout the article, $\Omega \subset \mathbb{R}^2$ will denote a bounded Lipschitz domain. We let $\nu_{\partial\Omega}$ denote the outward pointing unit normal along $\partial\Omega$.

Two spaces of vector fields that will play a prominent role in our analysis are $BV(\Omega;\mathbb{R}^2)$, the space of vector fields of bounded variation taking values in $\mathbb{R}^2$, and $H_{\mathrm{div}}(\Omega;\mathbb{R}^2)$, the Hilbert space of $L^2(\Omega;\mathbb{R}^2)$ vector fields having weak L^2 divergence. We will often be interested in vector fields that lie in the intersection of these spaces, and are in addition $\mathbb{S}^1$-valued.

We recall that a map $u \in BV(\Omega,\mathbb{R}^2)$ is approximately continuous in $\Omega\backslash J_u$, where J_u is the jump set of u and is countably 1-rectifiable. By rectifiability, we note that J_u is contained in an at most countable union of C^1 curves up to an $\mathcal{H}^1$ null set, where $\mathcal{H}^1$ denotes a one-dimensional Hausdorff measure. We fix a regular orientation of these C^1 curves that contain almost all of J_u, and let (τ_u,ν_u) denote the approximate unit tangent and unit normals to J_u that respect this orientation. Denoting the half planes

$$H^{\pm}_{\nu_u(x)} := \{y \in \mathbb{R}^2 : (y-x)\cdot\nu_u(x) \gtrless 0, \text{ resp., } \leqslant 0\},$$

u admits traces along J_u. That is, there exist two measurable functions $u_\pm$ on J_u such that for $\mathcal{H}^1$-a.e. $x \in J_u$, we have

$$\lim_{r\downarrow 0}\frac{1}{r^2}\int_{Q_r(x,\nu_u(x))\cap H^{\pm}_{\nu_u(x)}} |u(y)-u_\pm(x)|\,dy = 0,$$

with $Q_r(x,\nu_u(x))$ denoting the square of side length r, centered at x, that has one side parallel to $\nu_u(x)$.

Now, if $u \in BV \cap H_{\mathrm{div}}(\Omega;\mathbb{R}^2)$, then along the jump set J_u, an application of the Divergence Theorem shows that one must have $u_+(x)\cdot\nu_u(x) = u_-(x)\cdot\nu_u(x)$ for $\mathcal{H}^1$-a.e. $x \in J_u$. It follows that the jump in u along J_u is equal to the jump in the tangential component of u across J_u.

Concerning the space $H_{\mathrm{div}}(\Omega;\mathbb{R}^2)$, we recall that elements of $H_{\mathrm{div}}(\Omega;\mathbb{R}^2)$ have a well-defined normal trace on $\partial\Omega$, viewed as a distribution in the Sobolev space $H^{-1/2}(\partial\Omega)$; cf. [25, Chap. 1]. This distribution is defined by the integration-by-parts formula

$$\langle (u\cdot\nu_{\partial\Omega}),\phi\rangle := \int_\Omega \nabla\Phi\cdot u\,dx + \int_\Omega (\operatorname{div} u)\Phi\,dx, \tag{2.1}$$

where $\phi \in H^{1/2}(\partial\Omega)$, and Φ is an $H^1(\Omega)$ extension of ϕ.

We will frequently be concerned with vector fields $u \in BV(\Omega;\mathbb{S}^1)\cap H_{\mathrm{div}}(\Omega;\mathbb{S}^1)$ satisfying $|u(x)| = 1$. For such vector fields, we in fact have that the distribution $u\cdot\nu$ is induced by an $L^\infty(\partial\Omega) = \big(L^1(\partial\Omega)\big)^*$ function. To see this, let $\phi \in (2.1)$ be an $L^1(\partial\Omega)$ function, and let $\Phi \in W^{1,1}(\Omega)$ denote an extension of ϕ to Ω. We again define $\langle (u\cdot\nu_{\partial\Omega}),\phi\rangle$ by the formula (2.1). While linearity of $(u\cdot\nu)$ is immediate, its

continuity follows by applications of the Hölder and Sobolev embedding inequalities. It can be checked by an approximation argument that this definition is independent of the extension Φ of ϕ.

For a given $g \in H^{1/2}(\Omega;\mathbb{R}^2)$, we will also denote by $H^1_g(\Omega;\mathbb{R}^2)$ the Sobolev space of H^1 vector-valued functions having trace g on $\partial\Omega$.

3. Compactness and partial Γ-convergence on a general domain. We begin our rigorous analysis with the following compactness theorem for energy bounded sequences.

THEOREM 3.1 (compactness). *Assume* $\{v_\varepsilon\} \subset H^1(\Omega;\mathbb{R}^2)$ *satisfies the uniform energy bound*

$$\sup_{\varepsilon>0} E_\varepsilon(v_\varepsilon) < \infty.$$

Then there exists a subsequence (still denoted here by v_ε*) and a function* $v \in H_{\rm div}(\Omega;\mathbb{S}^1)$ *such that*

$$v_\varepsilon \rightharpoonup v \quad \text{in } H_{\rm div}(\Omega;\mathbb{R}^2), \tag{3.1}$$

$$v_\varepsilon \to v \quad \text{in } L^2(\Omega;\mathbb{R}^2). \tag{3.2}$$

We will write $v_\varepsilon \overset{\wedge}{\rightharpoonup} v$ when both (3.1) and (3.2) hold. Property (3.1) is immediate in light of the uniform bound on the L^2-norm of the divergence, while (3.2) follows from the proof of [12, Prop. 1.2]. The hypotheses of this proposition from [12] differ from our setting in that their sequence is assumed to be divergence-free, whereas ours has the weaker assumption of a uniform L^2 bound on the divergence. However, a minor modification of their proof allows for accommodation of this weaker assumption.

Before proceeding, we wish to stress that a uniform energy bound does *not* allow one to conclude that the limit lies in $BV(\Omega;\mathbb{S}^1)$; see the discussion on [4, pp. 338–340] or Remark 6.3 below. Our partial Γ-convergence result in this section, however, is phrased with this extra assumption. To this end, we fix boundary data $g \in H^{1/2}(\partial\Omega;\mathbb{S}^1)$ for admissible functions in E_ε. We point out that for a sequence $\{u_\varepsilon\} \subset H^1(\Omega;\mathbb{R}^2)$ satisfying $u_\varepsilon \cdot \nu_{\partial\Omega} = g \cdot \nu_{\partial\Omega}$, under the topology $u_\varepsilon \overset{\wedge}{\rightharpoonup} u$ with u assumed to lie in $BV(\Omega,\mathbb{S}^1) \cap H_{\rm div}(\Omega,\mathbb{S}^1)$, it follows that

$$u_{\partial\Omega}(x) \cdot \nu_{\partial\Omega}(x) = g(x) \cdot \nu_{\partial\Omega} \quad \text{for } \mathcal{H}^1\text{-a.e. } x \text{ on } \partial\Omega. \tag{3.3}$$

Here we denote by $u_{\partial\Omega}$ its trace on $\partial\Omega$. Indeed, for any $\phi \in H^1(\Omega)$ the Divergence Theorem yields

$$\begin{aligned}\int_{\partial\Omega} u_{\partial\Omega} \cdot \nu_{\partial\Omega}\, \phi\, d\mathcal{H}^1(x) &= \int_\Omega \nabla\phi \cdot u\, dx + \int_\Omega \operatorname{div} u\, \phi\, dx \\ &= \lim_{\varepsilon\to 0} \int_\Omega \{\nabla\phi \cdot u_\varepsilon\, dx + \operatorname{div} u_\varepsilon\, \phi\}\, dx = \int_{\partial\Omega} g \cdot \nu_{\partial\Omega}\, \phi\, d\mathcal{H}^1(x).\end{aligned}$$

Now for any $u \in BV(\Omega,\mathbb{S}^1) \cap H_{\rm div}(\Omega,\mathbb{S}^1)$ such that $u_{\partial\Omega} \cdot \nu_{\partial\Omega} = g \cdot \nu_{\partial\Omega}$ on $\partial\Omega$ we define our candidate E_0 for the Γ-limit of E_ε via

$$E_0(u) := \frac{L}{2}\int_\Omega (\operatorname{div} u)^2\, dx + \frac{1}{6}\int_{J_u} |u_- - u_+|^3\, d\mathcal{H}^1 + \frac{1}{6}\int_{\partial\Omega} |u_{\partial\Omega} - g|^3\, d\mathcal{H}^1. \tag{3.4}$$

We remark that if one introduces the measurable function $X : J_u \to [0,\pi/2]$ by

$$X := \frac{1}{2}\min\left|\widehat{u_\pm, u_\mp}\right|$$

so that X denotes the minimal half-angle between the unit vectors u_+ and u_-, then the quantity $|u_- - u_+|$ arising in the Γ-limit can be equivalently expressed as $2\sin X$. Similarly one can express $|u_{\partial\Omega} - g|$ as $2\sin X_{\partial\Omega}$, where $X_{\partial\Omega} := \frac{1}{2}\min\left|\widehat{u_{\partial\Omega}, g}\right|$. Of course, for all $x \in \partial\Omega$ such that $u_{\partial\Omega} = g$, the last integral in (3.4) vanishes, whereas the condition that $|u_{\partial\Omega}| = 1$ along with (3.3) implies that whenever $u_{\partial\Omega}(x) \neq g(x)$, one necessarily has

$$|u_{\partial\Omega}(x) - g(x)| = 2\sqrt{1 - (g(x) \cdot \nu_{\partial\Omega}(x))^2}.$$

Similarly, another alternative to the expression $|u_-(x) - u_+(x)|$ is

$$|u_-(x) - u_+(x)| = 2\sqrt{1 - (u_+(x) \cdot \nu_u)^2} = 2\sqrt{1 - (u_-(x) \cdot \nu_u)^2},$$

where ν_u denotes the measure-theoretic normal to the jump set J_u.

The main result of this section is a Γ-convergence type of result relating E_ε to E_0 under the assumption of $BV(\Omega; \mathbb{S}^1)$ competitors for E_0.

THEOREM 3.2. *Let $u \in H_{\mathrm{div}}(\Omega; \mathbb{S}^1) \cap BV(\Omega; \mathbb{S}^1)$ with $u_{\partial\Omega} \cdot \nu_{\partial\Omega} = g \cdot \nu_{\partial\Omega}$.*

(i) *If $u_\varepsilon \in H^1_g(\Omega, \mathbb{R}^2)$ is a sequence of functions such that $u_\varepsilon \overset{\triangle}{\to} u$, then*

$$\liminf_{\varepsilon \to 0} E_\varepsilon(u_\varepsilon) \geqslant E_0(u). \tag{3.5}$$

(ii) *There exists $w_\varepsilon \in H^1_g(\Omega; \mathbb{R}^2)$ with $w_\varepsilon \overset{\triangle}{\to} u$ satisfying*

$$\limsup_{\varepsilon \to 0} E_\varepsilon(w_\varepsilon) = E_0(u). \tag{3.6}$$

Proof. (i) We begin with the argument for lower-semicontinuity (3.5). We base our argument on the corresponding result for the Aviles–Giga functional established in [5]. For a more self-contained treatment, we refer the reader to [15], where we pursue an approach more in the spirit of [3].

We suppose that $u_\varepsilon \overset{\triangle}{\to} u$ for $u \in BV(\Omega) \cap H_{\mathrm{div}}(\Omega; \mathbb{R}^2)$ with $|u(x)| = 1$ for a.e. $x \in \Omega$, and $u_{\partial\Omega} \cdot \nu_{\partial\Omega} = g \cdot \nu_{\partial\Omega}$ along $\partial\Omega$. We may also assume $\liminf_{\varepsilon\to 0} E_\varepsilon(u_\varepsilon) < \infty$, since otherwise the claim is trivial.

We will use the following notation:

$$e_\varepsilon(v) := \frac{1}{2}\left(\varepsilon|\nabla v|^2 + \frac{1}{\varepsilon}(|v|^2 - 1)^2 + L(\operatorname{div} v)^2\right).$$

Now we let J_u denote the jump set of the vector field u, and here, unlike in (3.4), we also include in our definition of J_u jumps on $\partial\Omega$ where the tangential component of u is minus that of g. By the rectifiability of J_u we can express J_u as

$$J_u = \left(\bigcup_{k=1}^{\infty} \Gamma_k\right) \cup \Gamma_0,$$

where Γ_k are C^1 embedded curves of finite Hausdorff measure and $\mathcal{H}^1(\Gamma_0) = 0$.

We now fix a number $\delta > 0$, and since $E_0(u) < \infty$, we can select an integer N_δ such that

$$\frac{1}{6}\int_{J_u} |u_- - u_+|^3 \, d\mathcal{H}^1 \leqslant \sum_{k=1}^{N_\delta} \frac{1}{6}\int_{\Gamma_k} |u_- - u_+|^3 \, d\mathcal{H}^1 + \delta. \tag{3.7}$$

We can always assume that $\overline{\Gamma}_k \cap \overline{\Gamma}_{k'} = \emptyset$ for $k \neq k'$, and then we denote by β_δ the minimal separation given by

$$\beta_\delta := \min_{k,k' \in \{1,2,\ldots,N_\delta\},\ k \neq k'} \operatorname{dist}\,(\overline{\Gamma}_k, \overline{\Gamma}_{k'}). \tag{3.8}$$

Then for each $k \in \{1, 2, \ldots, N_\delta\}$ we introduce an open neighborhood J_u^k of Γ_k via

$$J_u^k = \left\{ x \in \Omega : \operatorname{dist}(x, \Gamma_k) < \min\left\{ \frac{\beta_\delta}{2}, \frac{\delta}{\mathcal{H}^1(\Gamma_k) k^2} \right\} \right\}.$$

From (3.8) we see that these neighborhoods are disjoint, and we also note that $\left|J_u^k\right| \leqslant \frac{\delta}{k^2}$ so that

$$\left| \bigcup_{k=1}^{N_\delta} J_u^k \right| \leqslant C\delta, \tag{3.9}$$

where here $|\cdot|$ denotes Lebesgue measure.

Now

$$E_\varepsilon(u_\varepsilon) \geqslant \frac{L}{2} \int_{\Omega \setminus \cup_{k=1}^{N_\delta} J_u^k} (\operatorname{div} u_\varepsilon)^2 + \int_{\cup_{k=1}^{N_\delta} J_u^k} e_\varepsilon(u_\varepsilon)\, dx, \tag{3.10}$$

and by convexity and the resulting lower-semicontinuity, it follows that

$$\liminf_{\varepsilon \to 0} \int_{\Omega \setminus \cup_{k=1}^{N_\delta} J_u^k} (\operatorname{div} u_\varepsilon)^2\, dx \geqslant \int_{\Omega \setminus \cup_{k=1}^{N_\delta} J_u^k} (\operatorname{div} u)^2.$$

Hence, condition (3.5) will follow from (3.7) and (3.9) by letting δ approach 0 once we can establish that

$$\liminf_{\varepsilon \to 0} \int_{\cup_{k=1}^{N_\delta} J_u^k} e_\varepsilon(u_\varepsilon)\, dx \geqslant \sum_{k=1}^{N_\delta} \frac{1}{6} \int_{\Gamma_k} |u_- - u_+|^3\, d\mathcal{H}^1 - O(\delta). \tag{3.11}$$

Inequality (3.11) follows readily from the lower-semicontinuity argument given for the Aviles–Giga functional (AG) in [5, Thm. 3.2], once one accounts for the extra terms present in our model due to nonzero divergence. More precisely, we wish to apply the results in [5], where our vector fields u_ε play the role of $(\nabla u_\varepsilon)^\perp$ for the scalar-valued functions u_ε in [5].

In the argument of [5], crucial use is made of the Jin–Kohn entropy $\Xi : \mathbb{R}^2 \to \mathbb{R}^2$ given by

$$\Xi(v) := \left(\frac{1}{3} v_2^3 + v_2 v_1^2 - v_2, \frac{1}{3} v_1^3 + v_1 v_2^2 - v_1 \right) \quad \text{for } v = (v_1, v_2),$$

along with all of its rotations; cf. [19]. The version of Ξ given above is well suited to the situation where the jump set is parallel to one of the coordinate axes. One calculates that for any vector field v one has

$$\operatorname{div} \Xi(v) = (|v|^2 - 1)(\partial_x v_2 + \partial_y v_1) + 2 v_1 v_2 \operatorname{div} v. \tag{3.12}$$

It is the last term in this expression that drops in the setting of [5], and so in that case the divergence of the Jin–Kohn entropy is seen to bound the Aviles–Giga energy

(AG) from below after an application of the inequality $a^2+b^2 \geqslant 2ab$. For our energy, the same will be true once we apply this trivial inequality to both terms in (3.12), leading to the following slight modification:

$$\begin{aligned}
\operatorname{div}\Xi(v) &\leqslant \frac{1}{2}\left(\varepsilon(\partial_x v_2+\partial_y v_1)^2+\frac{1}{\varepsilon}(|v|^2-1)^2\right)+\frac{L}{2}(\operatorname{div} v)^2+\frac{2}{L}v_1^2v_2^2\\
&\leqslant \frac{1}{2}\left(\varepsilon\,|\nabla v|^2+\frac{1}{\varepsilon}(|v|^2-1)^2\right)+\frac{L}{2}(\operatorname{div} v)^2+\frac{2}{L}v_1^2v_2^2+\varepsilon\partial_x v_2\,\partial_y v_1\\
&= e_\varepsilon(v)+\frac{2}{L}v_1^2v_2^2-\varepsilon\operatorname{Jac} v+\varepsilon\partial_x v_1\partial_y v_2\\
&\leqslant e_\varepsilon(v)+\frac{2}{L}v_1^2v_2^2-\varepsilon\operatorname{Jac} v+\frac{\varepsilon}{2}(\operatorname{div} v)^2, \qquad (3.13)
\end{aligned}$$

where $\operatorname{Jac} v$ refers to the Jacobian $\det Dv$.

Applying (3.13) with $v=u_\varepsilon$ and using that $u_\varepsilon \overset{\triangle}{\to} u$, along with (3.9), we integrate over $\cup_{k=1}^{N_\delta} J_u^k$ and take liminf over ε to find that

$$\begin{aligned}
&\liminf_{\varepsilon\to 0}\int_{\cup_{k=1}^{N_\delta}J_u^k} e_\varepsilon(u_\varepsilon)\,dx\\
&\geqslant \liminf_{\varepsilon\to 0}\left\{\int_{\cup_{k=1}^{N_\delta}J_u^k}\operatorname{div}\Xi(u_\varepsilon)+\varepsilon\operatorname{Jac} u_\varepsilon-\frac{2}{L}{u_\varepsilon}_1^2{u_\varepsilon}_2^2-\frac{\varepsilon}{2}(\operatorname{div} u_\varepsilon)^2\,dx\right\}\\
&\geqslant \liminf_{\varepsilon\to 0}\int_{\cup_{k=1}^{N_\delta}J_u^k}\operatorname{div}\Xi(u_\varepsilon)\,dx-\liminf_{\varepsilon\to 0}\varepsilon\int_{\cup_{k=1}^{N_\delta}J_u^k}\operatorname{Jac} u_\varepsilon\,dx-C\delta. \qquad (3.14)
\end{aligned}$$

Here we have used the assumed uniform energy bound on $\{u_\varepsilon\}$ to see that $\lim_{e\to 0}\varepsilon\int_\Omega(\operatorname{div} u_\varepsilon)^2\,dx=0$. One shows that the term involving the Jacobian integral vanishes in the $\varepsilon\to 0$ limit via an integration by parts precisely as in the proof of [5, Thm. 3.2] (though in that setting it appears as a Hessian), and the liminf inequality of the divergence of the Jin–Kohn entropy, namely,

$$\liminf_{\varepsilon\to 0}\int_{\cup_{k=1}^{N_\delta}J_u^k}\operatorname{div}\Xi(u_\varepsilon)\,dx\geqslant\sum_{k=1}^{N_\delta}\frac{1}{6}\int_{\Gamma_k}|u_--u_+|^3\,d\mathcal{H}^1,$$

follows exactly as in that proof as well. This yields (3.11) and completes the proof of (3.5)

(ii) The proof of (3.6) follows the approach of [8] rather closely, and therefore we present only an outline of the argument, highlighting the steps that are different for our problem by focusing primarily on the treatment of the divergence term in the energies. To facilitate comparison with [8], we adopt the notation of that proof wherever possible.

(a) *Preparation.* We let $\phi:\mathbb{R}^2\to[0,1]$ be a smooth radially symmetric bump function with $\int\phi=1$ and $\operatorname{spt}(\phi)\subset B_1$. For any $\varepsilon>0$, we denote as usual $\phi_\varepsilon(\cdot):=\frac{1}{\varepsilon^2}\phi(\frac{\cdot}{\varepsilon})$ and set $u_\varepsilon:=u*\phi_\varepsilon$.

We next introduce a class of step functions. For any $x_0\in\mathbb{R}^2$, $\nu\in\mathbb{S}^1$, and $\theta\in\mathbb{R}$, we introduce the function

$$s_{x_0,\nu,\theta}(x):=(\cos\theta)\nu-\sin\theta H\big((x-x_0)\cdot\nu\big)\nu^\perp,$$

where $H(t)=1$ for $t>0$ and $H(t)=-1$ for $t<0$. We then let $\mathcal{S}_{x_0}$ denote the collection of all such step functions at x_0.

For u as in the statement of the theorem, we let $x_0 \in J_u$ be a point at which its approximate unit normal ν_u is defined, and we consider $s_{x_0} \in \mathcal{S}_{x_0}$ such that $s^{\pm}_{x_0} = u_{\pm}(x_0)$ and $\nu = \nu_u$. We point out that this choice of s depends on the given function u. To alleviate notation, therefore, we just denote one subscript rather than all three.

Fixing now $\varepsilon > 0$, $\eta > 0$, $k \geqslant 1$, and $\overline{\theta} > 0$, we define "good points" on the jump set $J^g(\overline{\theta}, k, \eta, \varepsilon)$ to be those $x_0 \in J_u$ such that the following hold:

• The step function s_{x_0} associated to x_0 satisfies $|\sin\theta| \geqslant \sin\overline{\theta}$, and

$$\|\nabla u\|(B_{2k\varepsilon}(x_0)) \geqslant k\varepsilon \sin\overline{\theta} \tag{3.15}$$

and

$$\frac{1}{|B_{2k\varepsilon}|}\int_{B_{2k\varepsilon}(x_0)} |u - s_{x_0}|\,dx \leqslant \eta. \tag{3.16}$$

• For the finitely many balls $B_\varepsilon(y) \subset B_{2k\varepsilon}(x_0)$ with $y\cdot\nu = x_0\cdot\nu$ and $(y-x_0)\cdot\nu^\perp \in 2\varepsilon\mathbb{Z}$, one has

$$\int_{B_\varepsilon(y)\cap J_u} |[u]|^3\,d\mathcal{H}^1 \geqslant |2\sin\theta|^3 2\varepsilon - \eta\varepsilon. \tag{3.17}$$

We denote $\Omega^g := \{x \in \Omega : \operatorname{dist}(x, J^g) < k\varepsilon/2\}$ and set $\Omega^{(\varepsilon)} := \{x \in \Omega : \operatorname{dist}(x, \partial\Omega) > \varepsilon\}$.

For any $A \subset \mathbb{R}^2$ and $w \in H^1(A)$, it is also convenient to introduce the notation

$$F_\varepsilon[w; A] := \int_A \varepsilon|\nabla w|^2 + \frac{1}{\varepsilon}(|w|^2 - 1)^2\,dx.$$

(b) *Estimates away from* Ω^g. In this step, we show

$$\operatorname{Lim} E_\varepsilon[u_\varepsilon; \Omega^{(\varepsilon)}\backslash\Omega^g] := \overline{\lim_{\overline{\theta}\downarrow 0}}\ \overline{\lim_{k\uparrow\infty}}\ \overline{\lim_{\eta\downarrow 0}}\ \overline{\lim_{\varepsilon\downarrow 0}}\ E_\varepsilon[u_\varepsilon; \Omega^{(\varepsilon)}\backslash\Omega^g] = \frac{L}{2}\int_\Omega (\operatorname{div} u)^2\,dx. \tag{3.18}$$

This statement is the analogue of [8, Prop. 1]. At its heart, the argument relies on a scale-invariant Poincaré inequality, which asserts that for any $\delta > 0$, denoting $v_\delta := v * \phi_\delta$, we have

$$\left(\int_{B_\delta} |v - v_\delta(0)|^2\,dx\right)^{1/2} \leqslant c\|Dv\|(B_\delta) \tag{3.19}$$

for every $v \in BV(B_\delta)$, where $c > 0$ is independent of δ. Immediate consequences of the Poincaré inequality are the following linear and quadratic estimates: for every $k \geqslant 1$, we have

$$\text{(linear)} \qquad F_\varepsilon[u_\varepsilon; B_{k\varepsilon}] \leqslant C\|Du\|(B_{2k\varepsilon}),$$

$$\text{(quadratic)} \qquad F_\varepsilon[u_\varepsilon; B_{k\varepsilon}] \leqslant \frac{C}{\varepsilon}\left(\|Du\|(B_{2k\varepsilon})\right)^2,$$

with the constant C being independent of ε, k. The proof of (3.18) proceeds by partitioning the set $\Omega^{(\varepsilon)}\backslash\Omega^g$ according to how $\|Du\|(B_{2k\varepsilon}(x))$ scales in $k\varepsilon$. On most of Ω, where the scaling is sublinear, one uses the quadratic estimate to show vanishing of the F_ε energy, while away from the jump set where the scaling of the total variation

measure $\|Du\|$ is linear or superlinear, one uses the linear estimate, along with fine properties of BV functions, to argue that once again the F_ε energy vanishes. We refer the reader to [8, Prop. 1] for further details.

(c) *Estimates within* Ω^g. Having shown that the energy of the mollification u_ε outside of the set Ω^g is asymptotically just the bulk divergence, we simply set our desired recovery sequence $w_\varepsilon := u_\varepsilon$ on $\Omega \backslash \Omega^g$. We next define w_ε in Ω^g in order to capture the wall energies in the limit. To this end, let $\mathcal{F}^j = \{B_{2k\varepsilon}(x_i^j)\}_i$ for $1 \leqslant j \leqslant N$ be N families of disjoint balls with $x_i^j \in J^g$ and the $B_{k\varepsilon}(x_i^j)$ cover Ω^g. Here N is a universal constant obtained from Besicovitch's covering theorem. For fixed k, let $\psi \in C_c^\infty(B_k)$ denote a smooth cut-off function such that $\psi \equiv 1$ on B_{k-1}. For every $\varepsilon > 0$, we define $\psi^\varepsilon \in C_c^\infty(B_{k\varepsilon})$ by the formula $\psi^\varepsilon(x) := \psi\big(\frac{x}{\varepsilon}\big)$.

Setting $v^0 := u$, we inductively define $\{v^j\}_{j=1,\dots,N}$ as follows. At the jth step, on the family of balls $\mathcal{F}^j$, we define

$$v^j(x) := \begin{cases} \big(1 - \psi_\varepsilon(x - x_i^j)\big)v^{j-1}(x) + \psi_\varepsilon(x - x_i^j)s_i^j(x) & \text{if } x \in B_{k\varepsilon}(x_i^j) \text{ for some } i, \\ v^{j-1}(x) & \text{otherwise.} \end{cases}$$

Here s_i^j is the simple function associated to u at x_i^j. Then set $v := v^N * \phi_\varepsilon$.

For every i, j we define R_i^j to be the largest rectangle of the form $a < (x - x_i^j) \cdot (\nu_j^i)^\perp < b, |(x - x_i^j) \cdot \nu| < \sqrt{k}\varepsilon$, where $a, b \in \mathbb{R}$ to be contained in the ball $B_{(k-2)\varepsilon}(x_i^j)$ without intersecting any ball $B_{(k+1)\varepsilon}(x_{i'}^{j'})$ with $j' > j$. Existence of such a rectangle is immediate; for the proof of uniqueness of the rectangle R_i^j, we refer the reader to the geometric argument in [8, Prop. 2]. The main estimates of the present step correspond to [8, Prop. 2]:

$$\operatorname{Lim}\, E_\varepsilon \left[v, \Omega^{(\varepsilon)} \backslash \bigcup_{i,j} R_i^j \right] = \frac{L}{2} \int_\Omega (\operatorname{div} u)^2 \, dx. \tag{3.20}$$

On each R_i^j one has $v = \phi_\varepsilon * s_i^j$ and

$$\operatorname{Lim}\, \frac{1}{6} \sum_{i,j} \int_{R_i^j \cap J_{s_i^j}} |[s_i^j]|^3 \, d\mathcal{H}^1 \leqslant \frac{1}{6} \int_{J_u} |u_+ - u_-|^3 \, d\mathcal{H}^1. \tag{3.21}$$

The proof of the assertions that $v = \phi_\varepsilon * s_i^j$ on R_i^j and of estimate (3.21) follows exactly as in [8]. The key idea is of course to use the fact that each x_i^j is a good point on the jump set, so that we can invoke (3.17). For any ball B_{il}^j of the type considered in (3.17), one has the estimate

$$2\varepsilon |2 \sin\theta|^3 \leqslant \int_{B_{ijl} \cap J_u} |[u]|^3 \, d\mathcal{H}^1 + \eta\varepsilon.$$

Since the balls B_{il}^j are disjoint, and $l \leqslant 2k$, we find using (3.15) that

$$\begin{aligned} \sum_{i,j} \int_{R_i^j \cap J_{s_i^j}} |[s_i^j]|^3 \, d\mathcal{H}^1 &\leqslant \sum_{ijl} \int_{B_{ij}^l \cap J_u} |[u]|^3 \, d\mathcal{H}^1 + \sum_{i,j} 2k\eta\varepsilon \\ &\leqslant \int_{\Omega \cap J_u} |[u]|^3 \, d\mathcal{H}^1 + \sum_{ij} \frac{2\eta}{\sin\overline{\theta}} \|\nabla u\|(B_{2k\varepsilon}(x_i^j)) \\ &\leqslant \int_{\Omega \cap J_u} |[u]|^3 \, d\mathcal{H}^1 + \frac{2N\eta}{\sin\overline{\theta}} \|\nabla u\|(\Omega), \end{aligned}$$

where once again N is the Besicovitch constant. The result (3.21) follows by applying Lim. We now turn to the proof of (3.20). In light of our work in step (b) above, it suffices to prove the estimates

$$\text{Lim } F_\varepsilon \left[v; \bigcup_{i,j} B_{(k+1)\varepsilon}(x_i^j) \backslash B_{(k-2)\varepsilon}(x_i^j) \right] = 0, \tag{3.22}$$

$$\text{Lim } F_\varepsilon \left[v, \bigcup_{i,j} B_{(k-2)\varepsilon}(x_i^j) \backslash R_i^j \right] = 0, \tag{3.23}$$

and

$$\text{Lim } \int_{\cup_{i,j} B_{(k+1)\varepsilon}(x_i^j)} (\operatorname{div} v)^2 \, dx = 0. \tag{3.24}$$

The proof of (3.22) is identical to the proof of [8, eqns. (4.3) and (4.4)] to which we refer the reader. We prove (3.24). A basic estimate in the proof of (3.22) used in [8] is the inequality

$$\frac{1}{|B_{2k\varepsilon}|} \int_{B_{2k\varepsilon}(x_i^j)} |v^J - s_i^j| \, dx \leqslant C\eta, \tag{3.25}$$

holding for each fixed i, j and each $J = 0, \ldots, N$. This inequality is proved by induction on J. By testing against arbitrary L^2 functions, it is easy to check that $\operatorname{div} s_i^j = 0$ for each i, j. Attributing each x in the union $\bigcup_{j=1}^N B_{(k+1)\varepsilon}(x_i^j)$ to the level j where $v(x)$ was last modified, i.e., to the largest j such that $x \in B_{(k+1)\varepsilon}(x_i^j)$ for some i in the jth family, we find inductively that

$$\begin{aligned}
\frac{1}{2} \int_{\bigcup_{i,j} B_{(k+1)\varepsilon}} (\operatorname{div} v)^2 \, dx &\leqslant \sum_{i,j} \int_{B_{k\varepsilon}(x_i^j)} \left| \nabla \psi_\varepsilon(x - x_i^j) \cdot (v^{j-1} - s_i^j) * \phi_\varepsilon \right|^2 \, dx \\
&\quad + \int_{B_{(k+1)\varepsilon}(x_i^j)} (\operatorname{div} v^{j-1} * \phi_\varepsilon)^2 \, dx \\
\text{(Young's inequality)} \quad &\leqslant \sum_{i,j} \int_{B_{k\varepsilon}(x_i^j)} \left| \nabla \psi_\varepsilon(x - x_i^j) \cdot (v^{j-1} - s_i^j) \right|^2 \, dx \\
&\quad + \int_{B_{(k+1)\varepsilon}(x_i^j)} (\operatorname{div} v^{j-1})^2 \, dx \\
\text{(proceeding inductively)} \quad &\leqslant N \sum_{i,j} \int_{B_{k\varepsilon}(x_i^j)} \frac{1}{\varepsilon^2} |v^{j-1} - s_i^j|^2 \, dx + N \int_{\Omega^g} (\operatorname{div} u)^2 \, dx \\
\text{(since } |v^j|, |s_i^j| \leqslant 1) \quad &\leqslant 8\pi N k^2 \sum_{i,j} \frac{1}{|B_{2k\varepsilon}|} \int_{B_{2k\varepsilon}(x_i^j)} |v^{j-1} - s_i^j| \, dx \\
&\quad + N \int_{\Omega^g} (\operatorname{div} u)^2 \, dx \\
\text{(by (3.25))} \quad &\leqslant 8\pi N k^2 \eta + N \int_{\Omega^g} (\operatorname{div} u)^2 \, dx.
\end{aligned}$$

Since the foregoing estimates are uniform in ε, we send $\varepsilon \downarrow 0$, $\eta \downarrow 0$, $k \uparrow \infty$, and $\overline{\theta} \downarrow 0$, in that order, to arrive at (3.24), where for the second integral we have applied the monotone convergence theorem.

(d) *Estimates within the rectangles.* Finally, it remains to modify the construction v from the preceding step within the boxes R_i^j. This step relies on the following claim.

Claim. There is a smooth function w_ε such that $w_\varepsilon = v$ outside R_i^j and

$$F_\varepsilon[w_\varepsilon; R_i^j] \leqslant \ell_{ij}\frac{1}{6}|2\sin\theta|^3 + C\varepsilon\left(\frac{1}{\overline{\theta}} + ke^{-\overline{\theta}\sqrt{k}}\right). \tag{3.26}$$

Here θ is the angle of the step function s_i^j and $\ell_{ij} = \mathcal{H}^1(J_{v^N} \cap R_i^j)$ the length of the rectangle. The proof of this claim follows by using a standard "Modica–Mortola" type of heteroclinic within the rectangle along with a linear interpolant as in step (c) to match the boundary conditions. Control on the divergence term follows as in step (c), and control of the remaining terms proceeds as in [8]. Briefly, within each rectangle, we have, using (3.17),

$$\begin{aligned} F_\varepsilon[w_\varepsilon; R_i^j] &\leqslant \frac{1}{6}|2\sin\theta|^3\mathcal{H}^1(J_u \cap R_i^j) + \frac{C\varepsilon}{\overline{\theta}} + C\varepsilon k e^{-\overline{\theta}\sqrt{k}} \\ &\leqslant \frac{1}{6}\int_{J_u\cap R_i^j} |[u]|^3\, d\mathcal{H}^1 + C\varepsilon + k\varepsilon\eta + \frac{C\varepsilon}{\overline{\theta}} + C\varepsilon k e^{-\overline{\theta}\sqrt{k}}. \end{aligned}$$

In the above estimate we have used the fact that the rectangle R_i^j contains no more than k disjoint balls of the type in (3.17), and that the sum of their diameters is at least $\mathcal{H}^1(J_{v^N} \cap R_i^j) - 4\varepsilon$. Summing over the rectangles R_i^j, we find using (3.15) that

$$F_\varepsilon[w_\varepsilon; R_i^j] \leqslant \frac{1}{6}\int_{J_u} |[u]|^3\, d\mathcal{H}^1 + \sum_{i,j}\left(\frac{C(\overline{\theta})}{k} + C(\overline{\theta})\eta + Ce^{-\overline{\theta}\sqrt{k}}\right)\|\nabla u\|(B_{2k\varepsilon}(x_i^j)).$$

Taking Lim, we complete the requisite estimates, and the proof of the recovery sequence construction follows now by a diagonalization procedure. ∎

4. Criticality conditions and solution via characteristics for the limiting energy E_0. We begin this section by identifying the free boundary problem satisfied by critical points of the limiting functional E_0; cf. (3.4). We will use the criticality conditions derived below to later construct critical points for specific domains Ω and with specific boundary data g.

THEOREM 4.1. *Consider any $u \in BV(\Omega, \mathbb{S}^1) \cap H_{\mathrm{div}}(\Omega, \mathbb{S}^1)$ such that $u_{\partial\Omega} \cdot \nu_{\partial\Omega} = g \cdot \nu_{\partial\Omega}$ on $\partial\Omega$. Denote by J_u its jump set. Then if the first variation of E_0 evaluated at u vanishes when taken with respect to perturbations compactly supported in $\Omega \setminus J_u$, one has the condition*

$$u^\perp \cdot \nabla \mathrm{div}\, u = 0 \text{ holding weakly on } \Omega\setminus J_u, \tag{4.1}$$

where $u^\perp = (-u_2, u_1)$.

Furthermore, if the first variation vanishes at u when taken with respect to perturbations that fix J_u and are supported within any ball centered at a smooth point of $J_u \cap \Omega$, and if the traces $\mathrm{div}\, u_+$ and $\mathrm{div}\, u_-$ are sufficiently smooth, then one has the condition

$$L\,[\mathrm{div}\, u] - 4\big(1 - (u\cdot\nu_u)^2\big)^{1/2}(u\cdot\nu_u) = 0 \text{ on } J_u \cap \Omega, \tag{4.2}$$

where $[\cdot] = \cdot_+ - \cdot_-$ represents the jump across J_u, and ν_u is the unit normal to J_u pointing from the $+$ side of J_u to the $-$ side.

Finally, a vanishing first variation of E_0, evaluated at u that allows for local perturbations of the jump set $J_u \cap \Omega$ itself, leads to the condition

$$(\operatorname{div} u_+)^2 - (\operatorname{div} u_-)^2 + (\operatorname{div} u_+ + \operatorname{div} u_-)'\,(u_+ \cdot \tau_u - u_- \cdot \tau_u) = \frac{8\kappa}{3L}\big(1-(u\cdot\nu_u)^2\big)^{1/2}\big(1+2\,(u\cdot\nu_u)^2\big) \text{ on } J_u\cap\Omega, \tag{4.3}$$

whenever J_u, u_+, and u_- are sufficiently smooth. Here κ denotes the curvature of J_u, and $(\operatorname{div} u_+ + \operatorname{div} u_-)'$ refers to the tangential derivative along the jump set.

COROLLARY 4.2. *Suppose u is smooth and critical for E_0 in the sense of (4.1). Then writing u locally in terms of a lifting as $u(x,y) = e^{i\theta(x,y)}$ and defining the scalar $v := \operatorname{div} u$, one has that (4.1) is equivalent to the following system for the two scalars θ and v:*

$$-\sin\theta\,\theta_x + \cos\theta\,\theta_y = v, \tag{4.4}$$

$$-\sin\theta\,v_x + \cos\theta\,v_y = 0. \tag{4.5}$$

Consequently, starting from any initial curve in Ω parametrized via $s \mapsto \big(x_0(s), y_0(s)\big)$ along which θ and v take values $\theta_0(s)$ and $v_0(s)$, respectively, the characteristic curves, say $t \mapsto \big(x(s,t),\, y(s,t)\big)$, are given by

$$x(s,t) = \frac{1}{v_0(s)}\Big[\cos\big(v_0(s)t+\theta_0(s)\big) - \cos\theta_0(s)\Big] + x_0(s), \tag{4.6}$$

$$y(s,t) = \frac{1}{v_0(s)}\Big[\sin\big(v_0(s)t+\theta_0(s)\big) - \sin\theta_0(s)\Big] + y_0(s), \tag{4.7}$$

whenever $v_0(s) \neq 0$. The corresponding solutions $\theta(s,t)$ and $v(s,t)$ are given by

$$\theta(s,t) = v_0(s)t + \theta_0(s), \quad v(s,t) = v_0(s), \tag{4.8}$$

so that the characteristics are circular arcs of curvature $v_0(s)$ and carry constant values of the divergence. In case the divergence vanishes somewhere along the initial curve, i.e., $v_0(s) = 0$, then the characteristic is a straight line.

Proof of Theorem 4.1. We consider $u \in BV(\Omega,\mathbb{S}^1) \cap H_{\operatorname{div}}(\Omega,\mathbb{S}^1)$ such that $u_{\partial\Omega}\cdot\nu_{\partial\Omega} = g\cdot\nu_{\partial\Omega}$ on $\partial\Omega$. Then

$$\begin{aligned} E_0(u+\delta u) - E_0(u) = {} & \frac{L}{2}\int_\Omega \Big[(\operatorname{div} u + \operatorname{div}\delta u)^2 - (\operatorname{div} u)^2\Big]\,dx \\ & + \frac{1}{6}\int_{J_{u+\delta u}} |\,(u_- + \delta u_-) - (u_+ + \delta u_+)\,|^3\,d\mathcal{H}^1 - \frac{1}{6}\int_{J_u} |u_- - u_+|^3\,d\mathcal{H}^1 \\ & + \frac{1}{6}\int_{\partial\Omega\cap J_{u+\delta u}} |u_{\partial\Omega} + \delta u_{\partial\Omega} - g|^3\,d\mathcal{H}^1 \\ & - \frac{1}{6}\int_{\partial\Omega\cap J_u} |u_{\partial\Omega} - g|^3\,d\mathcal{H}^1 + \frac{1}{2}\int_\Omega \lambda\left(|u+\delta u|^2 - |u|^2\right)dx \end{aligned} \tag{4.9}$$

for any δu in $BV(\Omega,\mathbb{R}^2) \cap H_{\operatorname{div}}(\Omega,\mathbb{R}^2)$. The Lagrange multiplier λ in (4.9) enforces the constraint $u \in \mathbb{S}^1$.

We suppose first that the perturbation δu is either supported away from J_u or else is supported in a ball containing only a smooth portion of $J_u \cap \Omega$ and leaves the

jump set unaltered, i.e., $J_{u+\delta u} = J_u$. We recall that the normal component of any vector field $w \in H_{\mathrm{div}}(\Omega, \mathbb{S}^1)$ is continuous across the jump set of w and $|w_- - w_+| = 2\sqrt{1-(w\cdot\nu_u)^2}$. We have from (4.9) that

(4.10)
$$\delta E_0(u) = L\int_\Omega \operatorname{div} u \operatorname{div}\delta u\,dx - 4\int_{J_u\cap\Omega}\big(1-(u\cdot\nu_u)^2\big)^{1/2}(u\cdot\nu_u)(\delta u\cdot\nu_u)\,d\mathcal{H}^1 + \int_\Omega \lambda(u\cdot\delta u) = \int_\Omega [-L\nabla\operatorname{div} u + \lambda u]\cdot\delta u\,dx + \int_{J_u\cap\Omega}\Big[L\,(\operatorname{div} u_+ - \operatorname{div} u_-) - 4\big(1-(u\cdot\nu_u)^2\big)^{1/2}(u\cdot\nu_u)\Big](\delta u\cdot\nu_u)\,d\mathcal{H}^1.$$

From the consideration of perturbations δu supported away from J_u we conclude that u satisfies the equation

$$-L\nabla\operatorname{div} u + \lambda u = 0 \text{ in } \Omega\backslash J_u, \tag{4.11}$$

which is equivalent to (4.1). Then allowing for perturbations that meet $J_u\cap\Omega$ but that leave the jump set unaltered, we see that u is subject to the natural boundary conditions (4.2).

Before deriving the last condition (4.3) of the theorem, we wish to reinterpret the criticality condition (4.1) as a system of conservation laws. To this end, we suppose an $\mathbb{S}^1$-valued vector field u is critical in the sense of (4.1) and that we locally write u in terms of a lifting as $u(x,y) = e^{i\theta(x,y)}$. Assuming u is sufficiently smooth, we introduce the scalar $v := \operatorname{div} u$ and find that (4.1) is equivalent to the following system for the two scalars θ and v:

$$-\sin\theta\,\theta_x + \cos\theta\,\theta_y = v, \tag{4.12}$$

$$-\sin\theta\,v_x + \cos\theta\,v_y = 0. \tag{4.13}$$

Starting from any initial curve in Ω parametrized via $s\mapsto\big(x_0(s), y_0(s)\big)$ along which θ and v take values $\theta_0(s)$ and $v_0(s)$, respectively, one readily solves (4.12)–(4.13) to obtain (4.6), (4.7), and (4.8). We will exploit this property of constant divergence along these circular characteristics in a construction below.

Now we consider a competitor u that is critical in the sense of (4.1)–(4.2) and is such that within some ball $B\subset\Omega$ centered on a point of smoothness of $J_u\cap\Omega$ one has the following conditions: (i) $\operatorname{div} u$ is continuous on both sides of $J_u\cap B$, and (ii) the traces of $\operatorname{div} u$ on J_u are differentiable along $J_u\cap B$ with integrable derivatives. We let J_w be a small perturbation of $J_u\cap B$, where a part of a smooth curve in J_u is replaced by another smooth curve (Figure 4.1). We assume that the new curve maintains the connectivity of J_u, connects smoothly to J_u, and lies on one side of the original curve. Here, to fix ideas, we assume that J_w lies on the left side of J_u corresponding to u_+. We construct the perturbation w of u as follows. Supposing that on the right side of J_u the function w coincides with u_-, we use the characteristics on the right side of J_u, using u_- as initial values, to extend u_- into the interior of the region $J_w\triangle J_u$ thus defining w in that region (Figure 4.2). The characteristics extension of u_- into $J_w\triangle J_u$ allows us to maintain control over $\operatorname{div} w_- - \operatorname{div} u_-$ in that region.

We let Ω_w^+ denote the region to the left of J_w in Figure 4.1 and denote by w_- the trace of w on J_w as the boundary is approached from within the region $\operatorname{int}(J_w\triangle J_u)$.

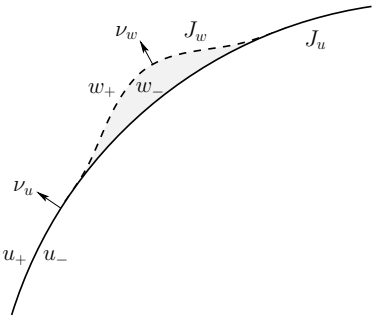

FIG. 4.1. *Perturbation of the jump set.*

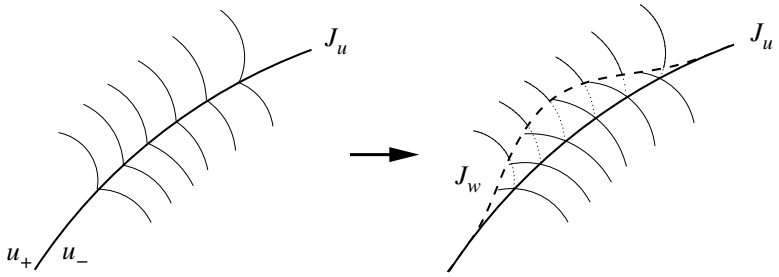

FIG. 4.2. *Construction of the perturbed minimizer w. The circular arcs of the characteristics defining u meet at the jump set J_u (left). The characteristics on the right side of J_u are used to extend u_- into the interior of the region $J_w \triangle J_u$ (right). In order to satisfy the continuity condition on J_w for the normal component of w, a small perturbation is added to u on the left side of J_w (not shown). The smallness of this perturbation is guaranteed by the continuity of u and its divergence on both sides of J_u.*

In order to make sure that the function w is in $H_{\mathrm{div}}(\Omega, \mathbb{S}^1)$, it must have the trace

$$w_+ = (2\nu_w \otimes \nu_w - I)\, w_- \tag{4.14}$$

on J_w as J_w is approached from within the region Ω_w^+. Indeed, as long as (4.14) holds, we have $w_+ \cdot \nu_w = w_- \cdot \nu_w$ and $(\nu_w \otimes \nu_w - I)\, w_+ = -(\nu_w \otimes \nu_w - I)\, w_-$.

We take advantage of the continuity of u and $\operatorname{div} u$ away from J_u, which ensures that the difference between w_+ as defined in (4.14) and u on J_w is small. In particular, if $u = e^{i\theta_u}$ to the left of J_u and $w_+ = e^{i\theta_{w_+}}$ on J_w, then $\delta\theta_+ = \theta_u - \theta_{w_+}$ is small on J_w. We introduce a small perturbation $\delta\theta$ compactly supported in Ω_w^+ and such that the trace of $\delta\theta$ on J_w is $\delta\theta_+$. Then we set $w = e^{i(\theta_u + \delta\theta)}$ in Ω_w^+ so that $w \in BV(\Omega, \mathbb{S}^1) \cap H_{\mathrm{div}}(\Omega, \mathbb{S}^1)$. Further, if we let $\delta u := w - u$, then $\delta u \in BV(\Omega_{w_+}, \mathbb{R}^2) \cap H_{\mathrm{div}}(\Omega_{w_+}, \mathbb{R}^2)$ is a small, complex-valued perturbation compactly supported in the closure of Ω_w^+.

Next, we suppose that J_u has the arc-length parametrization $r_u(s)$, where $s \in I$. We introduce the function $h : I \to \mathbb{R}$ with small C^1-norm such that h vanishes along with its derivatives at the endpoints of I. We now assume that $r_w(s) = r_u(s) + h(s)\nu_u(s)$ for $s \in I$ defines J_w. We let $\tau_u(s) = r_u'(s)$ so that $\nu_u(s) = \tau_u^\perp$.

By our assumptions on divergence and using the characteristics construction of u and w, it follows that $\|\delta u\|_{1,\infty} = O(\|h\|_{1,\infty})$. To simplify the notation, we assume that all equivalences in the derivation of the criticality condition appearing below up to (4.19) are true up to terms of order $O\left(\|h\|_{1,\infty}^2\right)$.

Integrating by parts and using (4.11), we have

$$\frac{L}{2}\int_{\Omega_w^+}\left\{(\operatorname{div} w)^2-(\operatorname{div} u)^2\right\}\,dx = L\int_{\Omega_w^+}\operatorname{div} u\operatorname{div}\delta u\,dx$$
$$= -L\int_{J_w\setminus J_u}(\operatorname{div} u)\,\delta u\cdot\nu_w\,d\mathcal{H}^1,$$

where ν_w is the unit normal to J_w pointing into Ω_w^+ (see Figure 4.1). The variation of the energy is then given by

$$E_0(w)-E_0(u) = \frac{L}{2}\int_{\operatorname{int}(J_w\triangle J_u)}\left\{(\operatorname{div} w)^2-(\operatorname{div} u)^2\right\}\,dx \tag{4.15}$$
$$-L\int_{J_w\setminus J_u}(\operatorname{div} u)\,\delta u\cdot\nu_w\,d\mathcal{H}^1+\frac{4}{3}\int_{J_w\setminus J_u}\left(1-(w\cdot\nu_w)^2\right)^{3/2}d\mathcal{H}^1$$
$$-\frac{4}{3}\int_{J_u\setminus J_w}\left(1-(u\cdot\nu_u)^2\right)^{3/2}d\mathcal{H}^1.$$

We estimate the third term in (4.15) as follows. Because

$$|r_w'| = |(1-h\kappa)\tau_u+h'\nu_u| = \sqrt{(1-h\kappa)^2+(h')^2} = 1-h\kappa$$

and

$$\nu_w = \frac{(1-h\kappa)\,\nu_u-h'\tau_u}{|(1-h\kappa)\tau_u+h'\nu_u|} = \nu_u-h'\tau_u,$$

we have

$$\begin{aligned}1-(w\cdot\nu_w)^2 &= 1-\left(w(r_u)+h\,\nabla w(r_u)\,\nu_u\right)\cdot(\nu_u-h'\tau_u)\big)^2\\ &= 1-\left(w(r_u)\cdot\nu_u+h\,\nabla w(r_u)\,\nu_u\cdot\nu_u-h'\tau_u\cdot w(r_u)\right)^2\\ &= 1-(w(r_u)\cdot\nu_u)^2-2\,(w(r_u)\cdot\nu_u)\,(h\,\nabla w(r_u)\,\nu_u\cdot\nu_u-h'\tau_u\cdot w(r_u))\end{aligned}$$

on $J_w\setminus J_u$ so that

$$\begin{aligned}&\frac{4}{3}\left(1-(w\cdot\nu_w)^2\right)^{3/2}\Big|_{J_w\setminus J_u}\\ &\quad=\frac{4}{3}\left(1-(w(r_u)\cdot\nu_u)^2-2\,(w(r_u)\cdot\nu_u)\,(h\,\nabla w(r_u)\,\nu_u\cdot\nu_u-h'\tau_u\cdot w(r_u))\right)^{3/2}\\ &\qquad=\frac{4}{3}\left(1-(w(r_u)\cdot\nu_u)^2\right)^{3/2}\\ &\qquad-4\left(1-(w(r_u)\cdot\nu_u)^2\right)^{1/2}(w(r_u)\cdot\nu_u)\,(h\,\nabla w(r_u)\,\nu_u\cdot\nu_u-h'\tau_u\cdot w(r_u))\\ &\qquad=\frac{4}{3}\left(1-(u\cdot\nu_u)^2\right)^{3/2}\\ &\qquad-4\left(1-(u\cdot\nu_u)^2\right)^{1/2}(u\cdot\nu_u)\,(h\,\nabla u_-\,\nu_u\cdot\nu_u-h'u_-\cdot\tau_u)\end{aligned}$$

for $s \in I$. With the help of (4.2), we conclude that

$$\begin{aligned}(4.16)\quad &\frac{4}{3}\int_{J_w\setminus J_u}\left(1-(w\cdot\nu_w)^2\right)^{3/2}d\mathcal{H}^1=\frac{4}{3}\int_I\left(1-(w\cdot\nu_w)^2\right)^{3/2}(1-h\kappa)\,ds\\ &=\frac{4}{3}\int_I\left(1-(u\cdot\nu_u)^2\right)^{3/2}(1-h\kappa)\,ds+L\int_I(\operatorname{div}u_+-\operatorname{div}u_-)\,\nabla u_-\,\nu_u\cdot\nu_u\,h\,ds\\ &\qquad+L\int_I\{(\operatorname{div}u_+)\,(u_+\cdot\tau_u)+(\operatorname{div}u_-)\,(u_-\cdot\tau_u)\}\,h'\,ds,\end{aligned}$$

because $w(r_u)\cdot\tau_u=-u_+\cdot\tau_u=u_-\cdot\tau_u$ on J_u. Similarly,

$$\begin{aligned}(4.17)\quad &-L\int_{J_w\setminus J_u}(\operatorname{div}u)\,\delta u\cdot\nu_w\,d\mathcal{H}^1\\ &\qquad=-L\int_I(\operatorname{div}u(r_w))\,(w_-(r_w)\cdot\nu_w-u(r_w)\cdot\nu_w)\,ds\\ &\qquad\quad=-L\int_I(\operatorname{div}u_+)\,(w(r_u)+h\,\nabla w(r_u)\,\nu_u\\ &\qquad\qquad-u_+-h\,\nabla u_+\,\nu_u)\cdot(\nu_u-h'\tau_u)\,ds\\ &\qquad\quad=L\int_I(\operatorname{div}u_+)\,(\nabla u_+\,\nu_u-\nabla u_-\,\nu_u)\cdot\nu_u\,h\,ds\\ &\qquad\qquad\qquad-L\int_I(\operatorname{div}u_+)\,(u_+\cdot\tau_u-u_-\cdot\tau_u)\,h'\,ds,\end{aligned}$$

since $w(r_u)\cdot\nu_u=u\cdot\nu_u$ on J_u. Adding (4.16) and (4.17), we find

$$\begin{aligned}(4.18)\quad &-L\int_{J_w\setminus J_u}(\operatorname{div}u)\,\delta u\cdot\nu_w\,d\mathcal{H}^1+\frac{4}{3}\int_{J_w\setminus J_u}\left(1-(w\cdot\nu_w)^2\right)^{3/2}d\mathcal{H}^1\\ &\qquad=\frac{4}{3}\int_I\left(1-(u\cdot\nu_u)^2\right)^{3/2}(1-h\kappa)\,ds\\ &\qquad+L\int_I\{(\operatorname{div}u_+)\,\nabla u_+\,\nu_u\cdot\nu_u-(\operatorname{div}u_-)\,\nabla u_-\,\nu_u\cdot\nu_u\}\,h\,ds\\ &\qquad\qquad-L\int_I\{(\operatorname{div}u_+)\,(u_+\cdot\tau_u)-(\operatorname{div}u_-)\,(u_-\cdot\tau_u)\}\,h'\,ds.\end{aligned}$$

Finally, changing the coordinates $(x,y)=r_u(s)+t\,h\,\nu_u(s)$ and using our continuity assumptions, we have for the first integral in (4.15) that

$$\begin{aligned}(4.19)\quad &\frac{L}{2}\int_{\operatorname{int}(J_w\triangle J_u)}\left\{(\operatorname{div}w)^2-(\operatorname{div}u)^2\right\}\,dx=\frac{L}{2}\int_I\int_0^h\left\{(\operatorname{div}w)^2-(\operatorname{div}u)^2\right\}(1-h\,\kappa)\,dt\,ds\\ &=\frac{L}{2}\int_I\int_0^h\left\{(\operatorname{div}u_-)^2-(\operatorname{div}u_+)^2\right\}\,dt\,ds=\frac{L}{2}\int_I\left\{(\operatorname{div}u_-)^2-(\operatorname{div}u_+)^2\right\}\,h\,ds.\end{aligned}$$

Equation (4.15), along with (4.18) and (4.19), gives the following variation of the

energy functional:

$$\begin{aligned}\delta E_0(u) = \frac{L}{2}\int_I \left\{(\operatorname{div} u_-)^2 - (\operatorname{div} u_+)^2\right\} h\,ds - \frac{4}{3}\int_I \left(1-(u\cdot\nu_u)^2\right)^{3/2} h\kappa\,ds \\ + L\int_I \left\{(\operatorname{div} u_+)\,\nabla u_+\,\nu_u\cdot\nu_u - (\operatorname{div} u_-)\,\nabla u_-\,\nu_u\cdot\nu_u\right\} h\,ds \\ - L\int_I \left\{(\operatorname{div} u_+)\,(u_+\cdot\tau_u) - (\operatorname{div} u_-)\,(u_-\cdot\tau_u)\right\} h'\,ds.\end{aligned} \tag{4.20}$$

Now, observe that the identities

$$\nabla u\,\nu_u\cdot\nu_u = \operatorname{div} u - \nabla u\,\tau_u\cdot\tau_u$$

and

$$(u\cdot\tau_u)' = \nabla u\,\tau_u\cdot\tau_u + \kappa\, u\cdot\nu_u$$

hold separately for u_- and u_+ on J_u. Substituting these expressions into (4.20) and integrating by parts, we have

$$\begin{aligned}\delta E_0(u) = \frac{L}{2}\int_I \left\{(\operatorname{div} u_+)^2 - (\operatorname{div} u_-)^2\right\} h\,ds - \frac{4}{3}\int_I \left(1-(u\cdot\nu_u)^2\right)^{3/2} h\,\kappa\,ds \\ - L\int_I \left\{(\operatorname{div} u_+)\nabla u_+\,\tau_u\cdot\tau_u - (\operatorname{div} u_-)\,\nabla u_-\,\tau_u\cdot\tau_u\right\} h\,ds \\ - L\int_I \left\{(\operatorname{div} u_+)\,(u_+\cdot\tau_u) - (\operatorname{div} u_-)\,(u_-\cdot\tau_u)\right\} h'\,ds \\ = \frac{L}{2}\int_I \left[(\operatorname{div} u_+)^2 - (\operatorname{div} u_-)^2\right] h\,ds - \frac{4}{3}\int_I \left(1-(u\cdot\nu_u)^2\right)^{3/2} h\,\kappa\,ds \\ - L\int_I \left\{(\operatorname{div} u_+)\,((u_+\cdot\tau_u)' - \kappa\,u\cdot\nu_u) - (\operatorname{div} u_-)\,((u_-\cdot\tau_u)' - \kappa\,u\cdot\nu_u)\right\} h\,ds \\ + L\int_I \left\{(\operatorname{div} u_+)'\,(u_+\cdot\tau_u) - (\operatorname{div} u_-)'\,(u_-\cdot\tau_u)\right\} h\,ds \\ + L\int_I \left\{(\operatorname{div} u_+)\,(u_+\cdot\tau_u)' - (\operatorname{div} u_-)\,(u_-\cdot\tau_u)'\right\} h\,ds\end{aligned} \tag{4.21}$$

for any smooth, positive h with a compact support in I. The same expression can be established for smooth, negative h with a compact support in I by considering perturbations of the jump set that lie on the right side of J_u. From this we immediately conclude that J_u is stationary whenever

$$\begin{aligned}(\operatorname{div} u_+)^2 - (\operatorname{div} u_-)^2 + (\operatorname{div} u_+ + \operatorname{div} u_-)'\,(u_+\cdot\tau_u - u_-\cdot\tau_u) \\ = \frac{8\kappa}{3L}\left(1-(u\cdot\nu_u)^2\right)^{3/2} - 2\kappa\,(\operatorname{div} u_+ - \operatorname{div} u_-)\,(u\cdot\nu_u) \text{ on } J_u.\end{aligned} \tag{4.22}$$

With the help of (4.2), the condition (4.22) can also be expressed as in (4.3). ∎

5. Results for the special case of a disc or an annulus. Now we present some examples where we take Ω to be a disc or an annulus. For the disc we will discuss three choices of boundary data $g : \partial\mathbb{D} \to \mathbb{S}^1$. Our focus is on optimizing the Γ-limit E_0 where we recall the normal component of competitors $u \in H_{\operatorname{div}}(\mathbb{D};\mathbb{S}^1)\cap BV(\mathbb{D};\mathbb{S}^1)$ is required to satisfy $u_{\partial\mathbb{D}}\cdot\nu_{\partial\mathbb{D}} = g_{\partial\mathbb{D}}\cdot\nu$ on $\partial\mathbb{D}$. Our discussion on the annulus is a

bit more formal, and we present examples that indicate situations where the wall is potentially curved, possibly occurring along the boundary.

Throughout this section, $\widehat{e}_r := (x,y)/\sqrt{x^2+y^2}$ denotes the unit radial vector field, while

$$\widehat{e}_\theta := (-y,x)/\sqrt{x^2+y^2}$$

denotes the unit angular vector field.

5.1. Tangential boundary conditions: $g(x,y) = (-y,x)$. In this case, a minimizer is clearly given by the divergence-free vector field

$$u(x,y) = \widehat{e}_\theta,$$

since for this choice of u one has $E_0(u) = 0$.

From the characteristics viewpoint laid out in the preceding section, this critical point is composed of characteristics which are simply radii through the origin of $\mathbb{D}$ to the boundary, corresponding to $v \equiv 0$ on each of these characteristics. We point out that for the Aviles–Giga energy, the authors in [18] classify zero energy states of the Aviles–Giga energy. More recently, [22] provides a quantitative version of the result in [18]. Another quantitative result with relevance to the Aviles–Giga energy was obtained in [21].

5.2. Hedgehog boundary conditions: $g(x,y) = (x,y)$. Here we can again precisely determine the minimizers of E_0.

THEOREM 5.1. *For $\Omega = \mathbb{D}$ and boundary data $g = (x,y)$ the two functions $u_*^\pm := r\widehat{e}_r \pm \sqrt{1-r^2}\widehat{e}_\theta$ are the only minimizers of the problem*

$$\inf E_0(u)$$

taken over competitors $u \in H_{\mathrm{div}}(\mathbb{D};\mathbb{S}^1) \cap BV(\mathbb{D};\mathbb{S}^1)$ satisfying $u_{\partial\mathbb{D}} \cdot \nu_{\partial\mathbb{D}} = g \cdot \nu_{\partial\mathbb{D}} = 1$ on $\partial\mathbb{D}$.

Proof. We note first that since $u \cdot \nu \equiv 1$ on $\partial\mathbb{D}$ and $|u| = 1$, necessarily competitors must have traces satisfying $u = g(x,y) = (x,y)$ along $\partial\mathbb{D}$.

Now given any competitor u, an application of the Cauchy–Schwarz and the Divergence Theorem gives

$$E_0(u) \geqslant \frac{L}{2}\int_{\mathbb{D}} (\operatorname{div} u)^2\,dx \geqslant \frac{L}{2}\frac{1}{\pi}\left(\int_{\mathbb{D}} \operatorname{div} u\,dx\right)^2 = 2\pi L = E_0(u_*^\pm). \tag{5.1}$$

Hence $u_*^\pm$ are minimizers, and any other minimizing competitor would have to yield equality in both of the inequalities above. Consequently, the only possible candidates for minimizers u must satisfy $J_u = \emptyset$ so that $u \in W^{1,1}(\mathbb{D})$ and $\operatorname{div} u \equiv$ *constant*. The Divergence Theorem and the boundary conditions then imply that in fact $\operatorname{div} u \equiv 2$ throughout $\mathbb{D}$.

Now we expand the competitor u in a Fourier series as

$$u = \sum_{n\in\mathbb{Z}} u_n(r)e^{in\theta},$$

where $u_n(r) = f_n(r) + ig_n(r)$ is a sequence of complex-valued functions that satisfy $u_0(1) = 1$ and $u_n(1) = 0$ if $n \neq 1$. In order to compute the divergence of u written in

the Fourier development, we write $V_n(r,\theta) := u_n(r)e^{in\theta}$ and note that, written as a vector field in $\mathbb{R}^2$, we have

$$V_n(r,\theta) = \begin{pmatrix} f_n(r)\cos n\theta - g_n(r)\sin n\theta \\ g_n(r)\cos n\theta + f_n(r)\sin n\theta \end{pmatrix}.$$

A calculation then yields that

$$\operatorname{div} V_n = \left(f_n'(r) + \frac{nf_n(r)}{r}\right)\cos(n-1)\theta - \left(g_n'(r) + \frac{ng_n(r)}{r}\right)\sin(n-1)\theta.$$

Using Plancherel and arguing as in (5.1), we find

$$E_0(u) = \frac{L}{2}\sum_n \int_{\mathbb{D}} (\operatorname{div} V_n)^2\,dx \geqslant \frac{L}{2}\int_{\mathbb{D}} (\operatorname{div} V_0)^2\,dx \geqslant 2\pi L,$$

and so $u = V_0 = u_0$ with necessarily $\operatorname{div} V_0 = f_0' + \frac{f_0}{r} \equiv 2$. Solving this ODE with the boundary condition $f_0(1) = 1$, we find $f_0(r) = r$, and since $|u| = 1$, it follows that $g_0(r) = \pm\sqrt{1-r^2}$ so that $u = u_*^+$ or u_-^+. ∎

5.3. Degree -1 boundary conditions: $g(x,y) = (x/R, -y/R)$. In this section, we develop a solution of the Euler–Lagrange boundary value problem (4.1)–(4.2) with the symmetries hinted at by a numerical solution of the relaxed problem. Although we do not claim that our construction yields a minimizer of the limiting functional, the minimizing property of our solution seems plausible given its close resemblance to the numerics, at least for a certain range of parameters of the problem.

We used the COMSOL Multiphysics finite elements software [1] to solve the Euler–Lagrange equation associated with the energy functional (1.1) in the circle of the radius $R = 0.6$, subject to the boundary conditions $g(x,y) = (x/R, -y/R)$. The (local) minimizers in COMSOL were found by simulating the gradient flow for E_ε on time intervals that were sufficiently large for a solution to reach an equilibrium. The results for $L = 0.5$ and $\varepsilon = 0.005$ are shown in Figures 5.1–5.2.

First, we observe that (i) the jump set of the solution in Figure 5.1 consists of two straight lines inclined at 45° to the horizontal axis, and (ii) the solution is symmetric with respect to reflections about both these lines, as well as the vertical and horizontal axes. Along the lines of the jump set, the symmetry is such that the normal components from either side are equal, while the tangential components are equal in absolute value and opposite in sign. Further, (iii) on both axes, the solution vector is parallel to the axis itself, and (iv) Figure 5.2 indicates that the sum of the traces of the divergence of u on both sides of the jump set equals zero. The last observation is consistent with the required criticality condition (4.3) since the curvature of the jump set is zero. Thus, it would be sufficient to look for the solution of (4.1)–(4.2) in one-eighth of a circle of radius R, and then extend the construction to the rest of the circle via symmetry.

Let Ω be a sector of the circle of radius R, as depicted in Figure 5.3. We seek a solution u of (4.1)–(4.2) in the form (4.6)–(4.8), where

$$J_u = \left\{(x,y) \in \mathbb{R}^2 : y = x, x \in \left(0, R/\sqrt{2}\right)\right\},$$

subject to the Dirichlet boundary conditions

$$u = (1,0) \text{ when } y = 0 \quad \text{and} \quad u = (x/R, -y/R) \text{ when } x^2 + y^2 = R^2. \tag{5.2}$$

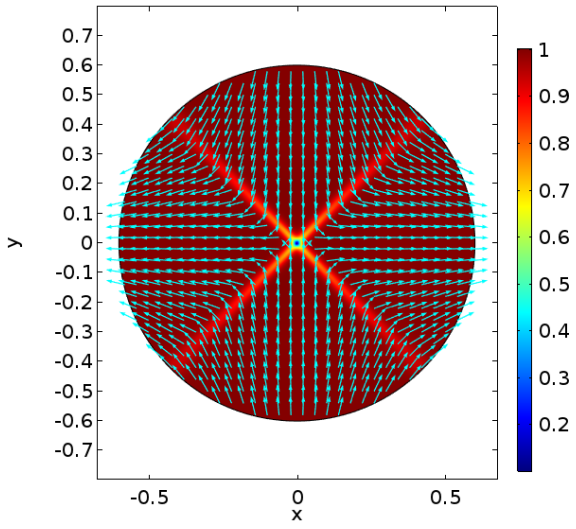

FIG. 5.1. *A solution u of the Euler–Lagrange equation associated with the energy functional* (1.1) *in the circle of the radius $R = 0.6$, subject to the boundary conditions $g(x, y) = (x/R, -y/R)$. Both u and $|u|$ are shown.*

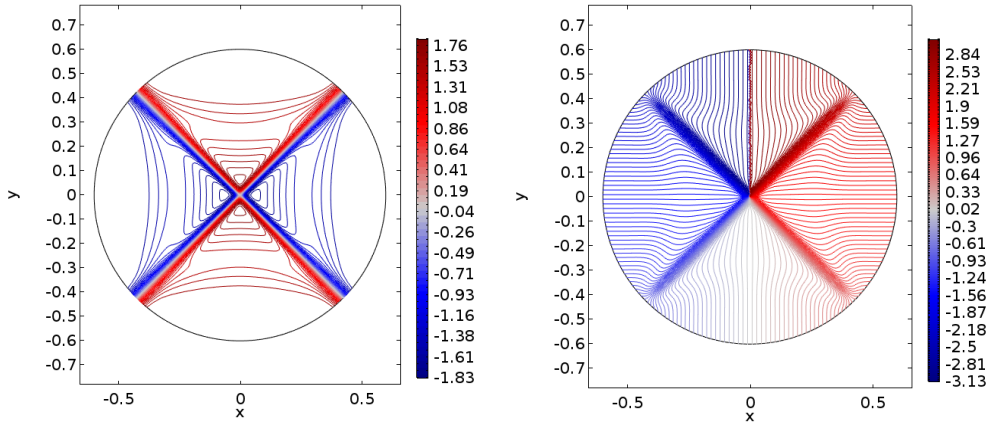

FIG. 5.2. *Level curves for the divergence of u (left) and for the angle θ (right), where $u = (\cos\theta, \sin\theta)$ is depicted in Figure* 5.1.

By our symmetry assumptions, the jump of $\operatorname{div} u$ on J_u is equal to $-2 \operatorname{div} u_-$, and hence (4.2) takes the form

$$L \operatorname{div} u - 2\left(1 - (u \cdot \nu_u)^2\right)^{1/2} (u \cdot \nu_u) = 0 \text{ on } J_u, \tag{5.3}$$

where we dropped the subscript "$-$" for notational convenience. Our last assumption is based on the behavior of the numerical solution in Figure 5.1. Considering the solution in the part of the disc corresponding to Ω in Figure 5.1 and recalling that $u = (\cos\theta, \sin\theta)$, in what follows we work with θ instead of u and assume that

$$\theta : \bar{\Omega} \to [-\pi/4, 0]\,. \tag{5.4}$$

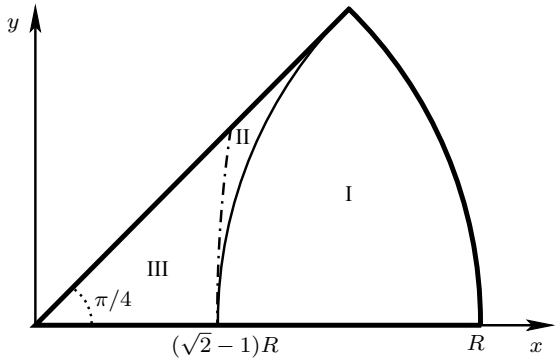

FIG. 5.3. *Regions corresponding to different characteristics families.*

We begin by identifying two distinct families of characteristics that originate on the x-axis and recover the solution of the limiting problem in regions I and III in Figure 5.3.

Step 1. First, taking into account (5.2), we construct a characteristic

$$(x(s,t), y(s,t), \theta(s,t), v(s,t))$$

with the initial data

$$(x(s,0), y(s,0), \theta(s,0), v(s,0)) = (s, 0, 0, v_0(s)) \text{ for } s \in [s_0, R],$$

which terminates at some point

$$(x\left(s, t^*(s)\right), y\left(s, t^*(s)\right)) = R\left(\cos\left(\psi\left(s, t^*(s)\right)\right), \sin\left(\psi\left(s, t^*(s)\right)\right)\right)$$

on the circular component of $\partial\Omega$ so that

$$\begin{aligned}(5.5)\quad &\left(x\left(s, t^*(s)\right), y\left(s, t^*(s)\right), \theta\left(s, t^*(s)\right), v\left(s, t^*(s)\right)\right)\\ &\quad = \left(R\cos\left(\psi\left(s, t^*(s)\right)\right), R\sin\left(\psi\left(s, t^*(s)\right)\right), -\psi\left(s, t^*(s)\right), v\left(s, t^*(s)\right)\right)\end{aligned}$$

for all $s \in [s_0, R]$. Here ψ represents the polar angle for a vector (x, y), while the parameter $s_0 > 0$ and the functions v_0 and t^* are all to be determined in the course of solving the problem. Note that, as a consequence of (4.12), the characteristics and the field u are mutually perpendicular at all points in Ω, and hence a characteristic intersecting the x-axis must be perpendicular to this axis at all points of intersection.

From (4.6)–(4.8), we conclude that

$$(5.6)\qquad x(s,t) = \frac{1}{v_0(s)}\left[\cos\big(\theta(s,t)\big) - 1\right] + t,$$

$$(5.7)\qquad y(s,t) = \frac{1}{v_0(s)}\sin\big(\theta(s,t)\big),$$

$$(5.8)\qquad \theta(s,t) = v_0(s)t,$$

$$(5.9)\qquad v(s,t) = v_0(s)$$

for all $s \in [s_0, R]$. Substituting $t^*(s)$ into these equations and using (5.5) gives

$$R\cos\left(\psi\left(s, t^*(s)\right)\right) = \frac{1}{v_0(s)}\left[\cos\big(\psi\left(s, t^*(s)\right)\big) - 1\right] + t,$$

$$R\sin\left(\psi\left(s,t^*(s)\right)\right) = -\frac{1}{v_0(s)}\sin\big(\psi\left(s,t^*(s)\right)\big), \tag{5.10}$$

$$\psi\left(s,t^*(s)\right) = -v_0(s)t^*(s)$$

for all $s \in [s_0, R]$. It follows from (5.10) that

$$v_0 \equiv -\frac{1}{R}$$

on $[s_0, R]$; that is, all characteristic curves that intersect both the x-axis and the circular part of the boundary are themselves arcs of circles of radius R, centered on the x-axis. These curves clearly foliate a region in Ω labeled by I in Figure 5.3 and bounded from the left by the mirror image of the boundary arc with respect to the line $x = R/\sqrt{2}$. The corresponding leftmost characteristic curve in family I will be denoted by $\boldsymbol{x}_r$. It intersects the x-axis at $x = (\sqrt{2}-1)R$ and is given by

$$x_r(t) = \sqrt{2}R - R\cos\big(t/R\big), \tag{5.11}$$

$$y_r(t) = R\sin\big(t/R\big), \tag{5.12}$$

$$\theta_r(t) = -t/R \tag{5.13}$$

for all $t \in [0, \pi R/4]$.

Step 2. Next, we turn our attention to the region labeled III in Figure 5.3. This region is foliated by the characteristic curves intersecting both the x-axis and jump set $J_u = \{(x,y) : y = x\}$. Because they originate on the x-axis, these characteristics are given for $s \in [0, s_0]$ by the same equations as in (5.6)–(5.9). For the remainder of this construction, we assume that $s \in [0, s_0]$. Suppose that intersection with the line $y = x$ occurs at some point $\left(x\left(s,t^*(s)\right), y\left(s,t^*(s)\right)\right)$. Then

$$x\left(s,t^*(s)\right) = y\left(s,t^*(s)\right), \tag{5.14}$$

$$Lv_0(t) + \cos^2\theta\left(s,t^*(s)\right) - \sin^2\theta\left(s,t^*(s)\right) = 0. \tag{5.15}$$

Here the second equation is the natural boundary condition (5.3) recast into a simpler form using trigonometric identities. Equation (5.15) along with (5.4) implies that

$$v_0(s) \leqslant 0. \tag{5.16}$$

From (5.6), (5.7), and (5.14), we obtain

$$\cos\theta\left(s,t^*(s)\right) - \sin\theta\left(s,t^*(s)\right) = 1 - sv_0(s). \tag{5.17}$$

Then (5.15) and (5.17) allow us to conclude that

$$\cos\theta\left(s,t^*(s)\right) + \sin\theta\left(s,t^*(s)\right) = -\frac{Lv_0(s)}{1-sv_0(s)}$$

and

$$2\cos\theta\left(s,t^*(s)\right) = 1 - tv_0(s) - \frac{Lv_0(s)}{1-sv_0(s)},$$

$$2\sin\theta\left(s,t^*(s)\right) = -1 + tv_0(s) - \frac{Lv_0(s)}{1-sv_0(s)}.$$

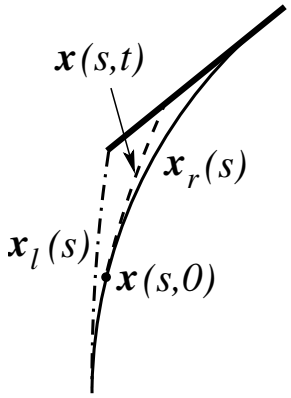

FIG. 5.4. *Characteristics construction in the intermediate region II.*

Hence

$$(1 - sv_0(s))^4 - 2(1 - sv_0(s))^2 + L^2 v_0^2(s) = 0$$

and

$$(1 - sv_0(s))^2 = 1 + \sqrt{1 - L^2 v_0^2(s)}. \tag{5.18}$$

Here the sign in front of the square root follows from (5.16). Now let

$$F(p) := (1 - tp)^2 - \sqrt{1 - L^2 p^2} - 1.$$

Clearly, F is continuous on $[-1/L, 0]$ for every $s \in [0, s_0]$ and

$$F(0) = -1 < 0 \qquad \text{and} \qquad F\left(-\frac{1}{L}\right) = \left(1 + \frac{s}{L}\right)^2 - 1 \geqslant 0.$$

Thus, there exists $-\frac{1}{L} \leqslant v_0(s) < 0$ such that (5.18) holds. Furthermore, by (5.18), we have the bound $1 - sv_0(s) < \sqrt{2}$, so that $v_0(s) > -(\sqrt{2} - 1)/s$, and, in particular,

$$v_0((\sqrt{2} - 1)R) > -\frac{1}{R}. \tag{5.19}$$

Note that the rightmost characteristic $\boldsymbol{x}_l$ in the family III originates from the same point $((\sqrt{2} - 1)R, 0)$ on the x-axis as the characteristic $\boldsymbol{x}_r$ in the family I, and both $\boldsymbol{x}_l$ and $\boldsymbol{x}_r$ are tangent to each other at $((\sqrt{2}-1)R, 0)$. Inequality (5.19) demonstrates that the radius of $\boldsymbol{x}_r$ is smaller than the radius of $\boldsymbol{x}_l$ and so there is a wedge-shaped region in Ω, labeled II in Figure 5.4, which is covered neither by the characteristics from the family I nor by the characteristics from the family III. In Step 3 below, we construct the third family of characteristics that extends the solution to region II.

We conclude this part of the construction by showing that the characteristics of the family III indeed foliate region III. We take the derivative of both sides of (5.18) with respect to s and solve for $v_0'(s)$ to obtain

$$v_0'(s) = -v_0(s)\left[s - \frac{L^2 v_0(s)}{2(1 - sv_0(s))\sqrt{1 - L^2 v_0^2(s)}}\right]^{-1} > 0.$$

It follows that the characteristic curves in region III are the circular arcs having curvature that increases with s. Since these curves also cross the x-axis at 90°, they completely cover region III without intersecting one another. We also note that $\lim_{s\to 0} v_0(s) = -\frac{1}{L}$, and so the divergence of our solution in region III remains bounded.

Step 3. Finally, we use characteristics to extend the solution to region II. The procedure is illustrated in Figure 5.4. We use the curve (5.11)–(5.13) as the initial data for the new family of characteristics. For the remainder of this section, we will assume that $s \in (0, \pi R/4)$. Let

$$\begin{aligned} x_0(s) &= \sqrt{2}R - R\cos\big(s/R\big),\\ y_0(s) &= R\sin\big(s/R\big),\\ \theta_0(s) &= -s/R. \end{aligned}$$

Then, from (4.6)–(4.8), we have that

$$x(s,t) = \frac{1}{v_0(s)}\left[\cos\big(\theta(s,t)\big) - \cos\big(s/R\big)\right] + \sqrt{2}R - R\cos\big(s/R\big), \tag{5.20}$$

$$y(s,t) = \frac{1}{v_0(s)}\left[\sin\big(\theta(s,t)\big) + \sin\big(s/R\big)\right] + R\sin\big(s/R\big), \tag{5.21}$$

$$\begin{aligned} \theta(s,t) &= v_0(s)t - s/R,\\ v(s,t) &= v_0(s). \end{aligned}$$

The new characteristic curves are still assumed to terminate on the jump set $y = x$, and hence they must satisfy conditions (5.14)–(5.15). Setting $\theta^*(s) = \theta(s, t^*(s))$ and simplifying, these conditions take the form

$$\cos\theta^*(s) - \sin\theta^*(s) = A(s), \tag{5.22}$$

$$\cos\theta^*(s) + \sin\theta^*(s) = -\frac{Lv_0(s)}{A(s)}, \tag{5.23}$$

where

$$A(s) := \sqrt{2}\left[(Rv_0(s)+1)\sin\big(s/R + \pi/4\big) - Rv_0(s)\right]. \tag{5.24}$$

The assumption (5.4) implies that

$$v_0(s) \leqslant 0 \quad \text{and} \quad A(s) > 0. \tag{5.25}$$

Following the same procedure as in Step 2, we find that $v_0(s)$ satisfies

$$A^2(s) = 1 + \sqrt{1 - L^2 v_0^2(s)}, \tag{5.26}$$

and hence

$$v_0(s) \geqslant -\frac{1}{L} \quad \text{and} \quad A(s) \leqslant \sqrt{2}. \tag{5.27}$$

The second inequality in (5.27) is equivalent to

$$v_0(s) \geqslant -\frac{1}{R}$$

and, combining this inequality with the first inequality in (5.25) and the first inequality in (5.27), we have

$$-\min\left\{\frac{1}{R},\frac{1}{L}\right\} \leqslant v_0(s) \leqslant 0. \tag{5.28}$$

Now, let

$$F(p) := 2\big[(Rp+1)\sin\big(s/R+\pi/4\big) - Rp\big]^2 - \sqrt{1-L^2p^2} - 1$$

and

$$q = \min\left\{\frac{1}{R},\frac{1}{L}\right\}.$$

Clearly, F is continuous on $[-q,0]$ for every $s \in (0,\pi R/4)$ and

$$F(0) = -2\cos^2\big(s/R+\pi/4\big) < 0,$$

while

$$F(-q) = \begin{cases} 2\big[(1-R/L)\sin\big(s/R+\pi/4\big) + R/L\big]^2 - 1 > 0, & L \geqslant R, \\ 1-\sqrt{1-(L/R)^2} > 0, & L < R. \end{cases}$$

This implies that there exists $v_0(s) \in (-q,0)$ such that (5.26) holds and, therefore, (i) v is uniformly bounded in region II, (ii) the inequality in (5.28) can be considered to be strict, and (iii) v experiences a jump on $\boldsymbol{x}_r$. Note that, at the same time, θ is continuous across $\boldsymbol{x}_r$ by construction.

It remains to show that the characteristic curves cover the entire region II, without intersecting each other. We begin by proving the following.

LEMMA 5.1. *The functions v_0 and θ^* are, respectively, strictly increasing and strictly decreasing on $(0,\pi R/4)$.*

Proof. Taking the derivative of both sides of (5.26) with respect to s, solving for $v_0'(s)$, and using (5.28), we determine that $v_0'(s) > 0$ for all $s \in (0,\pi R/4)$. This establishes monotonicity of v_0. Likewise, solving (5.22)–(5.23) for $\cos\theta^*$, taking the derivative with respect to s, and using the just established fact that the $v_0' > 0$ on $(0,\pi R/4)$, along with (5.24) and (5.28), proves that $\theta^{*\prime} < 0$ on $(0,\pi R/4)$. ∎

To demonstrate that no two characteristic curves can intersect, we suppose, by contradiction, that a circular arc of a characteristic C_1 intersects another circular arc of a characteristic C_2 before reaching $y = x$, where C_1 corresponds to $s = s_1$, whereas C_2 corresponds to $s = s_2$ with $s_1 < s_2$. Using (5.20), (5.21), and the monotonicity of v_0, we know that the curvature of C_1 is greater than the curvature of C_2. Since C_1 starts out (i.e., at $t = 0$) to the left of C_2, this intersection could not be merely tangential since a circle of larger curvature can't sit outside of a circle of smaller curvature. Thus, the intersection is transversal. Now the angle between an incoming characteristic and the line $y = x$ is the nonnegative angle $\theta^* + \pi/4$, and if the intersection is transversal, then necessarily $\theta^*(s_1) + \pi/4 < \theta^*(s_2) + \pi/4$, contradicting Lemma 5.1.

We end this section by plotting the analytical counterparts of Figure 5.2 obtained in MATLAB using the characteristics solutions constructed above.

Figure 5.5 should be compared to the solution in the sector in Figure 5.2, corresponding to the polar angle ranging between 0° and 45°. Regions I and II are clearly

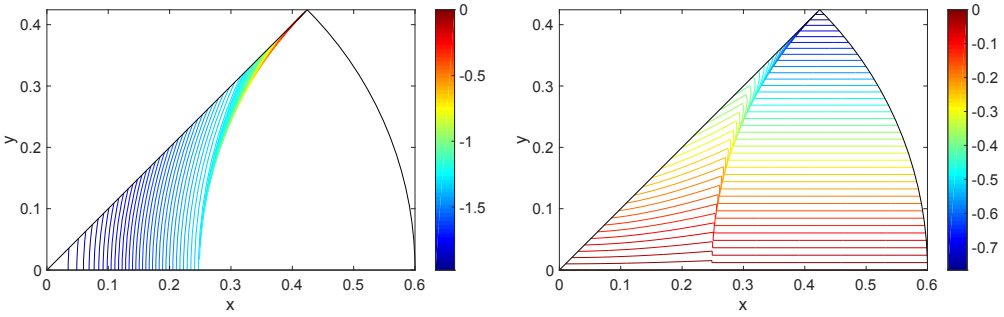

FIG. 5.5. *Level curves for the divergence of u (left) and for the angle θ (right), where $u = (\cos\theta, \sin\theta)$ is a solution obtained using characteristics. The divergence is constant in the empty region.*

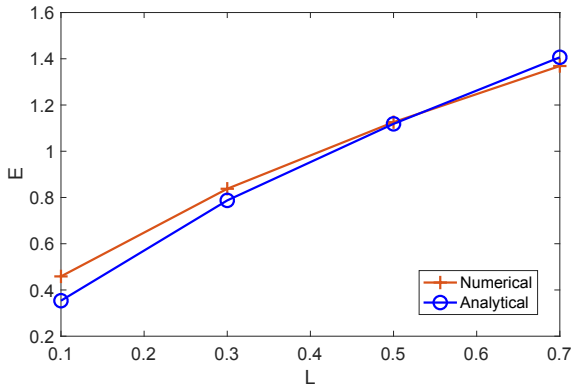

FIG. 5.6. *Energy of the critical point as a function of L.*

visible in Figure 5.2, and there is a good match between Figures 5.5 and 5.2 in these regions. The discrepancy between the solutions in region III can be attributed to the qualitative differences between minimizers of the ε-level and Γ-limit problems. The energies of the characteristics and numerical solutions are depicted in Figure 5.6 for a small range of L values. The plots demonstrate that both the numerical solution and the solution constructed using characteristics have energy increasing with L on $L \in [0.1, 0.7]$. The systematic difference between the graphs can once again be explained by the fact that the corresponding functions are critical points of the different energy functionals.

5.4. An example in an annulus: Curved walls. In this section we briefly outline an example where our analysis suggests that the jump set can occur along a portion of the boundary with a jump set, and might in general not be a straight line segment. For details of the calculations in this section, we refer the reader to [15].

We fix a number $R > 1$ and let Ω denote an annulus described in polar coordinates by $\Omega := \{1 < r < R\}$. For the boundary conditions g defined by $g(1,\theta) = -\widehat{e}_\theta$, $g(R,\theta) = \widehat{e}_\theta$, we study the problem of minimizing the E_0 energy among competitors $u_{\partial\Omega} \cdot \nu_{\partial\Omega} = g \cdot \nu_{\partial\Omega} = 0$. It is reasonable to expect that a minimizer is radial, so we work within the ansatz

$$u(r,\theta) = p(r)\widehat{e}_r + q(r)\widehat{e}_\theta, \tag{5.29}$$

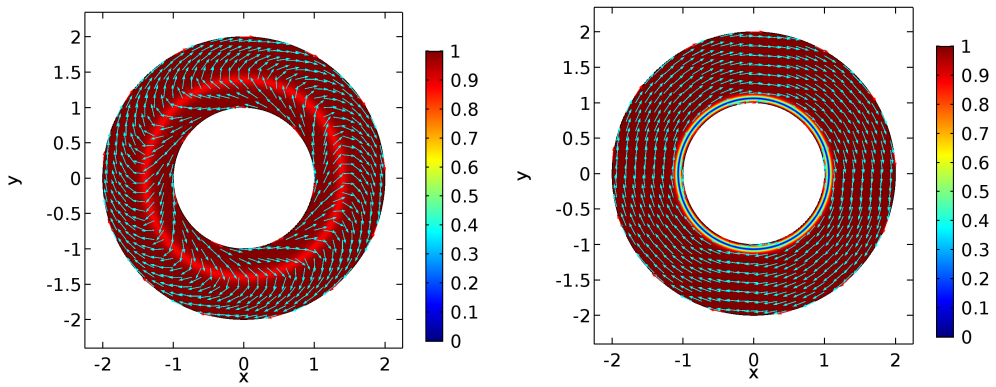

FIG. 5.7. *Energy minimizers in an annulus for $L = 0.2$ (left) and $L = 2$ (right). Here $\varepsilon = 0.03$ and the color represents $|u|$.*

where $p^2 + q^2 \equiv 1$, $p(1) = 0 = p(R)$. Within this ansatz, $\operatorname{div} u = \frac{1}{r}(rp(r))_r$, and the jump set is composed of a union of circles, possibly occurring at the boundary of Ω. Away from jumps, criticality of $\int(\operatorname{div} u)^2\,dx$ within this ansatz requires that $p(r)$ satisfies the ODE $\frac{\partial}{\partial r}\left(\frac{1}{r}\frac{\partial}{\partial r}(rp(r))\right) = 0$, so that $p(r)$ takes the form $p(r) = Cr + \frac{D}{r}$ for constants C, D. In the absence of a jump circle in Ω, the boundary conditions on p would force $p(r) \equiv 0$, and then either $q(r) \equiv 1$ or $q(r) \equiv -1$. This results in boundary walls, either along the circle $\rho = 1$ or along $\rho = R$, respectively, carrying energies $E_0(\hat{e}_\theta) = \frac{8\pi}{3}$ or $E_0(-\hat{e}_\theta) = \frac{8\pi R}{3}$.

Elementary calculations, detailed in [15], demonstrate that for any $R > 1$, for an interval of L-values of the form $(0, L_*(R))$, where $L_*(R) < \frac{8}{3}\frac{R^2-1}{R^2+1}\left(1 - \frac{\sqrt{2}R}{\sqrt{R^2+1}}\left(\frac{3}{4}\right)^{3/2}\right)$, the energy E_0 within the ansatz (5.29) has an internal wall with energy strictly smaller than $\frac{8\pi}{3}$, which is the energy associated to a boundary wall.

At the other extreme, we also show in [15] that for any fixed $R > 1$ and L sufficiently large depending on R, the minimizer of E_0 with these "mismatched" boundary conditions and the radial ansatz (5.29) necessarily has its wall at the inner boundary $\rho = 1$. The associated energy is $E_0(\hat{e}_\theta) = \frac{8\pi}{3}$.

In Figure 5.7, we illustrate observations made in this section by presenting the results of gradient flow simulations for the functional E_ε for two different values of L. For the smaller value of $L = 0.2$, the (local) minimizer has a shallower circular wall in the interior of the domain, while the minimizer for $L = 2$ has a deeper wall that coincides with the inner boundary of the annulus. Note that the simulations were done without assuming that competitors are radially symmetric—the apparent symmetry of minimizers suggests that it might be reasonable to consider the ansatz (5.29).

6. Results for the special case of a rectangle. In this section we pose the problem on a rectangle, taking $\Omega = (-T, T) \times (-H, H)$ for positive constants T and H. Furthermore, we specialize the boundary conditions on competitors $u : \Omega \to \mathbb{R}^2$ to be given by

$$u(x, \pm H) = \left(\pm\sqrt{1-a^2}, a\right) \text{ for } |x| \leqslant T, \quad u \text{ is } 2T\text{-periodic in } x, \tag{6.1}$$

for some constant $a \in [0, 1)$. The rationale for considering E_ε and the Γ-limit E_0 in this rather special setting is to focus on the structure of wall transitions in as

simple a situation as possible. A primary focus will be on examining the relative favorability of one-dimensional—that is, purely y-dependent structures—versus two-dimensional structures such as cross-ties that one associates with related models in micromagnetics; cf., e.g., [3]. Other goals we have in mind concerning this special case include better understanding the relative weights given to jump energy versus divergence for minimizers, as well as the possible emergence of periodic structures on a scale smaller than the fixed rectangle width $2T$.

6.1. Study of the problem in a rectangle within a one-dimensional ansatz. We begin our analysis of E_ε and E_0 on the rectangle subject to the boundary conditions (6.1) by first studying the variational problem among one-dimensional competitors, i.e., functions of y alone. More specifically, for $0 \leqslant |a| < 1$ we consider the space of admissible functions

$$\mathcal{A}^1(a) := \{u = u(y) \in H^1((-H,H);\mathbb{R}^2), u(\pm H) = \big(\pm\sqrt{1-a^2}, a\big)\}$$

and consider the variational problem

$$\min_{u\in\mathcal{A}^1(\alpha)} E_\varepsilon^{1D}(u), \tag{6.2}$$

where

$$E_\varepsilon^{1D}(u) := \frac{1}{2}\int_{-H}^{H} \varepsilon|u'|^2 + \frac{1}{\varepsilon}(|u|^2-1)^2 + L(u_2')^2\,dy. \tag{6.3}$$

The corresponding Γ-limit E_0^{1D} is now defined over the class

$$\begin{aligned}\mathcal{A}^0 := \{&u = (u_1,u_2) :\ u_1^3 \in BV\big((-H,H)\big),\ u_2 \in H^1\big((-H,H)\big),\\ &u^{(2)}(\pm H) = a,\ |u| = 1 \text{ a.e. } y\},\end{aligned} \tag{6.4}$$

where the boundary conditions on u_2 come from (3.3). Then E_0 from (3.4) takes the form

$$\begin{aligned}E_0^{1D}(u) =: \frac{L}{2}\int_{-H}^{H}(u_2')^2\,dy + 4/3\sum_{y_j\in J_{u_1}}\big(1-u_2^2(y_j)\big)^{3/2}\\ + \frac{1}{6}\Big|\,u_1(-H)+\sqrt{1-a^2}\Big|^3 + \frac{1}{6}\Big|\,u_1(H)-\sqrt{1-a^2}\Big|^3.\end{aligned} \tag{6.5}$$

Not surprisingly, in this one-dimensional setting we can prove a much stronger compactness statement than is possible in the two-dimensional setting of Theorem 3.1. Here we establish the following theorem.

THEOREM 6.1. *Let $u_\varepsilon = (u_\varepsilon^{(1)}, u_\varepsilon^{(2)}) \in \mathcal{A}^1(a)$ with $E_\varepsilon^{1D}(u_\varepsilon) \leqslant C$. Then, up to extraction of subsequences, one has $u_\varepsilon^{(1)} \to u_1$ in $L^3(-H,H)$ for some function u_1 such that $u_1^3 \in BV(-H,H)$ and one has $u_\varepsilon^{(2)} \to u_2$ in $C^{0,\gamma}$ for all $\gamma < 1/2$. Furthermore, $|(u_1,u_2)| = 1$ a.e.*

Proof. Precompactness of $\{u_\varepsilon^{(2)}\}$ in $C^{0,\gamma}(-H,H)$ for $\gamma < 1/2$ is clear from the uniform H^1 bound and Sobolev imbedding. The thrust of the rest of the proof will be to prove the statement about $\{u_\varepsilon^{(1)}\}$. To this end, we define

$$\psi_\varepsilon(y) := \int_{-u_\varepsilon^{(1)}}^{u_\varepsilon^{(1)}} \big(1-s^2-(u_\varepsilon^{(2)})^2\big)\,ds = 2u_\varepsilon^{(1)} - 2u_\varepsilon^{(1)}(u_\varepsilon^{(2)})^2 - \frac{2}{3}(u_\varepsilon^{(1)})^3.$$

Since we have a uniform L^4 bound on $u_\varepsilon^{(1)}$ from the energy bound $E_\varepsilon^{1D}(u_\varepsilon) \leqslant C$ it readily follows that ψ_ε is uniformly bounded in $L^1(-H,H)$. Now we estimate the total variation of ψ_ε. We have

$$\begin{aligned}\int_{-H}^{H} |\psi_\varepsilon'|\, dy &\leqslant 2\int_{-H}^{H} \left|1-|u_\varepsilon|^2\right| \left|u_\varepsilon^{(1)\,\prime}\right| dy + 4\int_{-H}^{H} \left|u_\varepsilon^{(1)} u_\varepsilon^{(2)}\right| \left|u_\varepsilon^{(2)\,\prime}\right| dy \\ &\leqslant \frac{1}{\varepsilon}\int_{-H}^{H} \left(1-|u_\varepsilon|^2\right)^2 dy + \varepsilon \int_{-H}^{H} \left|u_\varepsilon^{(1)\,\prime}\right|^2 dy + \int_{-H}^{H} \left((u_\varepsilon^{(1)})^4 + (u_\varepsilon^{(2)})^4\right) dy \\ &\quad + 2\int_{-H}^{H} (u_\varepsilon^{(2)\,\prime})^2\, dy < C.\end{aligned}$$

Concluding the desired compactness of $\{u_\varepsilon^{(1)}\}$ relies on an algebraic identity. Using the BV bound on $\{\psi_\varepsilon\}$, and passing to subsequences that we do not denote explicitly, we know that ψ_ε converges in L^1. We now show that $\{u_\varepsilon^{(1)}\}_{\varepsilon>0}$ is a Cauchy sequence in L^3. For any $0<\varepsilon<\delta$, we have

$$\frac{4}{3}\big((u_\varepsilon^{(1)})^3 - (u_\delta^1)^3\big) = \Big(\psi_\varepsilon - \psi_\delta\Big) - 2(1-|u_\varepsilon|^2)u_\varepsilon^{(1)} + 2(1-|u_\delta|^2)u_\delta^{(1)}.$$

Hence, using Cauchy–Schwarz we obtain

$$\begin{aligned}&\frac{4}{3}\int_{-H}^{H} \left|(u_\varepsilon^{(1)})^3 - (u_\delta^{(1)})^3\right| dy \\ &\leqslant \int_{-H}^{H} |\psi_\varepsilon - \psi_\delta|\, dy + \varepsilon^{1/3}\int_{-H}^{H} |u_\varepsilon^{(1)}|^2\, dy + \frac{1}{\varepsilon^{1/3}}\int_{-H}^{H} (1-|u_\varepsilon|^2)^2\, dy \\ &\quad + \delta^{1/3}\int_{-H}^{H} |u_\delta^{(1)}|^2\, dy + \frac{1}{\delta^{1/3}}\int_{-H}^{H} (1-|u_\delta|^2)^2\, dy.\end{aligned}$$

Since $\{u_\varepsilon^{(1)}\}$ is uniformly bounded in L^4 by the energy bound, we can invoke the L^1-convergence of $\{\psi_\varepsilon\}$ to find that

$$\int_{-H}^{H} \left|(u_\varepsilon^{(1)})^3 - (u_\delta^{(1)})^3\right| \leqslant o(1), \tag{6.6}$$

as $\delta \to 0$. Since $|a-b|^3 \leqslant 4|a^3-b^3|$, it follows that $\{u_\varepsilon^{(1)}\}$ is Cauchy in L^3, and has a limit in this space, denoted u_1. Denoting the limit of $u_\varepsilon^{(2)}$ by u_2, it follows from the energy bound that $u_1^2 + u_2^2 = 1$ a.e. in $(-H,H)$. Consequently, the limit of the ψ_ε satisfies

$$\psi_\varepsilon \to \frac{4}{3}(u_1)^3 \tag{6.7}$$

in L^1. By lower-semicontinuity of the BV norm under L^1-convergence, we conclude that

$$(u_1)^3 \in BV(-H,H).$$

It follows that one-sided limits of $(u_1)^3$ exist at all $y \in (-H,H)$. Combined with u_2 being continuous on the same interval, this implies that $|u_1,u_2| = 1$ everywhere on $(-H,H)$. ∎

In light of the preceding compactness result, Theorem 6.1, one can establish a full Γ-convergence result in this one-dimensional setting without an assumption on the limiting functions lying in BV. We have the following.

THEOREM 6.2. *Let $u \in \mathcal{A}^0$. Then*

(i) *for any sequence $u_\varepsilon \in \mathcal{A}^1(a)$ satisfying $u_\varepsilon \overset{\triangle}{\to} u$, we have*

$$\liminf_{\varepsilon\to 0} E_\varepsilon^{1D}(u_\varepsilon) \geqslant E_0^{1D}(u); \tag{6.8}$$

(ii) *there exists a sequence $w_\varepsilon \in \mathcal{A}^1(a)$ with $w_\varepsilon \overset{\triangle}{\to} u$ and*

$$\lim_{\varepsilon\to 0} E_\varepsilon^{1D}(w_\varepsilon) = E_0^{1D}(u). \tag{6.9}$$

A proof of this particular case of Theorem 3.2 is significantly simpler and more transparent in the key elements of the argument [15].

Remark 6.3. We recall that in Theorem 3.2 we made the assumption $u \in BV$. That this is not quite the optimal space can already be seen in this simpler one-dimensional setting where one can construct a limiting vector field $u = (u_1, u_2)$ with u_1 having a countable collection of jumps of size $(\frac{1}{k})_{k\in\mathbb{N}}$. Such a construction can be arranged to have finite E_0 energy, but necessarily has infinite BV norm. The preceding theorem, however, guarantees the existence of a recovery sequence for such a competitor.

This phenomenon is well known for Aviles–Giga; see the discussion in [4, pp. 338–340]. The counterexample there is very similar in spirit, but is understandably a bit more involved due to the constraint imposed by the eikonal equation.

Next we pursue an understanding of minimizers of the one-dimensional Γ-limit E_0^{1D}.

THEOREM 6.4. *For any $a \in (0,1)$ the problem*

$$\inf_{\mathcal{A}^0} E_0^{1D}(u)$$

has a unique solution $u^* = (u_1^*, u_2^*)$, where u_1^* has exactly one jump located at $y = 0$ and u_2^* is linear on the subintervals $[-H, 0]$ and $[0, H]$. More precisely, the components are given by the formulas

$$u_2^*(y) = \begin{cases} a + \frac{M-a}{H}(y+H), & y \in (-H, 0], \\ a + \frac{M-a}{H}(H-y), & y \in (0, H), \end{cases} \tag{6.10}$$

$$u_1^*(y) = \begin{cases} -\sqrt{1-(u_2^*)^2} & \text{for } y \in [-H, 0], \\ \sqrt{1-(u_2^*)^2} & \text{for } y \in (0, H], \end{cases} \tag{6.11}$$

where the constant $M = M(L, H, a) \in (a, 1)$ is the minimizer of the problem

$$\min_{m\in[-1,1]} \frac{L}{H}(m-a)^2 + \frac{4}{3}(1-m^2)^{3/2}. \tag{6.12}$$

In case $a = 0$, the nature of the minimizer depends on the ratio L/H. If $L/H < 2$, then the minimizer is again unique and has the one-jump structure given by (6.10)–(6.11) *and the infimum is $\frac{L}{H} - \frac{1}{12}\frac{L^3}{H^3}$. If $L/H > 2$, then the minimizer is any step function of the form*

$$u(y) = \begin{cases} (-1, 0) & \text{for } y \in (-H, y^*], \\ (1, 0) & \text{for } y \in (y^*, H), \end{cases}$$

where $y* \in [-H, H]$ is arbitrary and the infimum is $4/3$. If $L/H = 2$, the family of step functions and the solution given by (6.10)–(6.11) are all minimizers.

Proof. Let $u = (u_1, u_2)$ be any competitor in $\mathcal{A}^0$. We denote by J_u the jump set of u, which in the present one-dimensional setting corresponds simply to the jump set of u_1, combined with either $-H$ or H, or both if either $u_1(-H) \neq -\sqrt{1-a^2}$ or $u_1(H) \neq \sqrt{1-a^2}$. We will write $\bar{J}_u$ for the closure of J_u and define the number M_u via

$$M_u := \begin{cases} \max_{y \in \bar{J}_u} u_2(y) & \text{if } \bar{J}_u \neq \emptyset, \\ \max_{y \in [-H,H]} u_2(y) & \text{if } \bar{J}_u = \emptyset. \end{cases}$$

In light of the continuity of u_2 and the compactness of $\bar{J}_u$ we note that this maximum will always be achieved at at least one point $\bar{y} \in [-H, H]$. We now proceed with three cases.

Case 1. *$\bar{J}_u \neq \emptyset$ and M_u is achieved at $\bar{y} \in (-H, H)$.* We note that this case includes the possibility that $\bar{y} \notin J_u$ but is simply a limit point of a sequence of points $\{y_j\}$ in the jump set. In this case $|u_-(y_j) - u_+(y_j)| \to 0$, meaning that the difference between the left and right traces of u_1 approaches zero. Since these traces are also opposites of each other, necessarily $u_1(\bar{y}) = 0$, forcing $u_2(\bar{y}) = 1 = M_u$.

Whether or not this subcase of Case 1 occurs, we now consider the competitor $\bar{u} = (\bar{u}_1, \bar{u}_2)$, whose second component is given by

$$\bar{u}_2 = \begin{cases} a + \frac{M_u - a}{\bar{y} + H}(y + H) & \text{for } y \in [-H, \bar{y}], \\ a + \frac{M_u - a}{\bar{y} - H}(y - H) & \text{for } y \in (\bar{y}, H], \end{cases} \tag{6.13}$$

and whose first component is given by

$$\bar{u}_1 = \begin{cases} -\sqrt{1 - \bar{u}_2^2} & \text{for } y \in [-H, \bar{y}], \\ \sqrt{1 - \bar{u}_2^2} & \text{for } y \in (\bar{y}, H]. \end{cases} \tag{6.14}$$

We calculate that

(6.15)

$$\begin{aligned} E_0^{1D}(u) &\geqslant \frac{L}{2} \int_{-H}^{\bar{y}} (u_2')^2 \, dy + \frac{L}{2} \int_{\bar{y}}^{H} (u_2')^2 \, dy + \frac{4}{3}(1 - M_u^2)^{3/2} \\ &\geqslant \frac{L}{2(\bar{y} + H)} \left(\int_{-H}^{\bar{y}} u_2' \, dy \right)^2 + \frac{L}{2(H - \bar{y})} \left(\int_{\bar{y}}^{H} u_2' \, dy \right)^2 + \frac{4}{3}(1 - M_u^2)^{3/2} \\ &= \frac{L(M_u - a)^2}{2(\bar{y} + H)} + \frac{L(M_u - a)^2}{2(H - \bar{y})} + \frac{4}{3}(1 - M_u^2)^{3/2} \\ &= \frac{L}{2} \int_{-H}^{\bar{y}} (\bar{u}_2')^2 \, dy + \frac{L}{2} \int_{\bar{y}}^{H} (\bar{u}_2')^2 \, dy + \frac{4}{3}(1 - \bar{u}_2(\bar{y})^2)^{3/2} = E_0^{1D}(\bar{u}), \end{aligned}$$

by the Cauchy–Schwarz inequality, with the inequality being strict unless u_2 is linear on the subintervals $(-H, \bar{y})$ and $(\bar{y}, H)$. Furthermore, among competitors of the form (6.13)–(6.14), the second-to-last line of (6.15) reveals that the optimal choice is to have $\bar{y} = 0$ yielding a minimal energy within this class of competitors of the form

$$E_0^{1D}(\bar{u}) = \frac{L}{H}(M_u - a)^2 + \frac{4}{3}(1 - M_u^2)^{3/2}. \tag{6.16}$$

Case 2. *Suppose $\bar{J}_u = \emptyset$.* In this case u_1 is continuous with $u_1(\pm H) = \pm\sqrt{1-a^2}$. Hence there exists a point $y \in (-H, H)$ such that $u_1(y) = 0$, meaning that $u_2(y) = 1$.

Therefore in this case, $M_u = u_2(\bar{y}) = 1$ for some $\bar{y} \in (-H, H)$. Then consider the competitor $\bar{u} = (\bar{u}_1, \bar{u}_2)$ given by (6.13)–(6.14) with $M_u = 1$, so that now u_1 is continuous as well. The calculation leading to (6.15), absent the jump term, implies in this case that

$$E_0^{1D}(u) \geqslant E_0^{1D}(\bar{u})$$

with the minimal value

$$E_0^{1D}(\bar{u}) = \frac{L}{H}(1-a)^2. \tag{6.17}$$

Case 3. *Suppose* $\bar{J}_u \neq \emptyset$ *and either* $M_u = u_2(-H)$ *or* $M_u = u_2(H)$. In the first case, we have

$$\sqrt{1-a^2}E_0^{1D}(u) \geqslant \frac{1}{6}(u_1(-H) + \sqrt{1-a^2})^3 = \frac{4}{3}(1-a^2)^{3/2} = E_0^{1D}(\bar{u}), \tag{6.18}$$

where $\bar{u} \equiv (\sqrt{1-a^2}, a)$, while in the second case we have

$$E_0^{1D}(u) \geqslant \frac{1}{6}(u_1(H) - \sqrt{1-a^2})^3 = \frac{4}{3}(1-a^2)^{3/2} = E_0^{1D}(\bar{u}), \tag{6.19}$$

where $\bar{u} \equiv (-\sqrt{1-a^2}, a)$. Again the inequalities are sharp unless $u \equiv \bar{u}$.

Having exhausted all possibilities, we next observe that the optimal formula (6.17) from Case 2 corresponds to (6.16) with $M_u = 1$, and the optimal formulas (6.18) and (6.19) from Case 3 correspond to (6.16) with $M_u = a$. Hence, the minimal energy corresponds to the minimization (6.12). Clearly this minimum must occur for $m \in [0,1]$, and since for $a \in (0,1)$ the function

$$f(m) := \frac{L}{H}(m-a)^2 + \frac{4}{3}(1-m^2)^{3/2}$$

satisfies the conditions $f'(0) < 0$ and $f'(1) > 0$, the minimum occurs on $(0,1)$. The conclusion of the theorem for this case then follows. When $a = 0$, one finds that $f'(0) = 0$, and some elementary calculus yields the stated dichotomy depending on the ratio L/H. When $a \neq 0$, it can be checked by elementary arguments that the interior minimum is unique. ∎

Remark 6.5. The proof of Theorem 3.2 reveals that resolving the internal structure of walls for the E_0 energy at the $\varepsilon > 0$ level using a one-dimensional construction is asymptotically optimal. However, it is possible to also have two-dimensional recovery sequences with the same energy asymptotics. To see this, set $S := \{|x| < 1/2\}$ and define the map $u : \mathbb{R}^2 \to \mathbb{R}^2$, which is 1-periodic in the x-direction, by

$$u(x,y) = u(r\cos\theta, r\sin\theta) := \begin{cases} \left(\frac{1}{\sqrt{2}}, -\frac{1}{\sqrt{2}}\right), & S \cap \{0 \leqslant \theta \leqslant \frac{\pi}{4}\}, \\ (\sin\theta, -\cos\theta), & S \cap \{\frac{\pi}{4} \leqslant \theta \leqslant \frac{3\pi}{4}\}, \\ \left(\frac{1}{\sqrt{2}}, \frac{1}{\sqrt{2}}\right), & S \cap \{\frac{3\pi}{4} \leqslant \theta \leqslant \pi\}, \\ \left(-\frac{1}{\sqrt{2}}, \frac{1}{\sqrt{2}}\right), & S \cap \{\pi \leqslant \theta \leqslant \frac{5\pi}{4}\}, \\ (\sin\theta, -\cos\theta), & S \cap \{\frac{5\pi}{4} \leqslant \theta \leqslant \frac{7\pi}{4}\}, \\ \left(-\frac{1}{\sqrt{2}}, -\frac{1}{\sqrt{2}}\right), & S \cap \{\frac{7\pi}{4} \leqslant \theta < 2\pi\}, \end{cases}$$

extended to all of $\mathbb{R}$ by $u(x+1,y) = u(x,y)$ for all $x \in \mathbb{R}$. We compute the E_0 energy per unit length of the cross-tie map u, which is divergence-free. Across the walls $\{|x| \leqslant 1/2, y = 0\}$, the jump angle is $\pi/4$. Similarly, along the walls $\{|y| \leqslant 1/2, x =$

$1/2\}$ the jump angle is $\pi/4$. Finally there are walls $\{|y| > 1/2, x = 1/2\}$, along which the angle varies with y and is in fact equal to $\arctan\left(\frac{1}{2y}\right)$ at height y. Adding up these various jump energies yields the energy per unit length,

$$E_0(u;S) = \frac{4}{3}\left[2\left(\frac{1}{\sqrt{2}}\right)^3 + 2\int_{1/2}^{\infty} \frac{1}{(1+4y^2)^{3/2}}\,dy\right] = \frac{4}{3}\left[\frac{1}{\sqrt{2}} + 1 - \frac{1}{\sqrt{2}}\right] = \frac{4}{3}.$$

This construction can be scaled down to fit into walls replacing a heteroclinic connecting $(1,0)$ and $(-1,0)$. This observation is reported without details in [20] based on a private communication with S. Serfaty.

6.2. A two-dimensional construction with cross-ties. In this section we construct a critical point to E_0 by solving the free boundary problem (4.1)–(4.3). Here our particular interest is to find parameter regimes within which the one-dimensional minimizer from Theorem 6.4 fails to minimize the full two-dimensional problem (3.4). The main result of this section is as follows.

THEOREM 6.6. *Consider the minimization problem for E_0 in the rectangle $\Omega = (-T,T)\times(-H,H)$, subject to the boundary conditions* (6.1) *with $a = 0$. There exist constants $L_0 \approx 1.27$ and $L_1 \approx 2.14$ such that whenever $L/H \in (L_0, L_1)$ and $T = H\tilde{T}(L/H)$, where $\tilde{T}(L/H)$ solves* (6.30)*, we have*

$$\inf E_0(u) < 2T \inf_{\mathcal{A}^0} E_0^{1D}(u). \tag{6.20}$$

Here the infimum on the left is taken over all $u \in H_{\mathrm{div}}(\Omega;\mathbb{S}^1) \cap BV(\Omega;\mathbb{S}^1)$ such that $u\cdot\nu = 0$ on the top and on the bottom $y = \pm H$ and u is $2T$-periodic in x.

Remark 6.7. Given the energy functional (3.4) and the rectangular domain Ω in the statement of Theorem 6.6, it is easy to see that by setting

$$\tilde{x} = \frac{x}{H},\ \tilde{y} = \frac{y}{H},\ \tilde{E}_0 = \frac{E_0}{H}$$

the rescaled variational problem for $\tilde{E}_0$ contains two independent parameters: the aspect ratio $\tilde{T} = T/H$ and the scaled elastic constant L/H. Then setting $\tilde{u}(\tilde{x},\tilde{y}) = u(H\tilde{x}, H\tilde{y})$ for any admissible $u \in H_{\mathrm{div}}(\Omega;\mathbb{S}^1)\cap BV(\Omega;\mathbb{S}^1)$, assuming that $\tilde{T} = \tilde{T}(L/H)$, and writing explicitly the dependence of the energy on L and H, we find that

$$\frac{1}{2T}E_0(u,L,H) = \frac{1}{2\tilde{T}}\tilde{E}_0(\tilde{u}, L/H). \tag{6.21}$$

In other words, the energy per unit length along the x-axis is a function of the scaled elastic constant L/H only.

The proof of Theorem 6.6 relies on a construction of a two-dimensional critical point of E_0 that resembles cross-tie walls well known in micromagnetics research ([17, 3]; see also Remark 6.5). Our construction is motivated by the numerics, which we will now describe.

To find two-dimensional critical points of E_0, we used the finite element software COMSOL [1] to determine the solutions of the Euler–Lagrange equation for E_ε numerically. Here the (local) minimizers were found by simulating the gradient flow for E_ε on time intervals that were sufficiently large for a solution to reach an equilibrium.

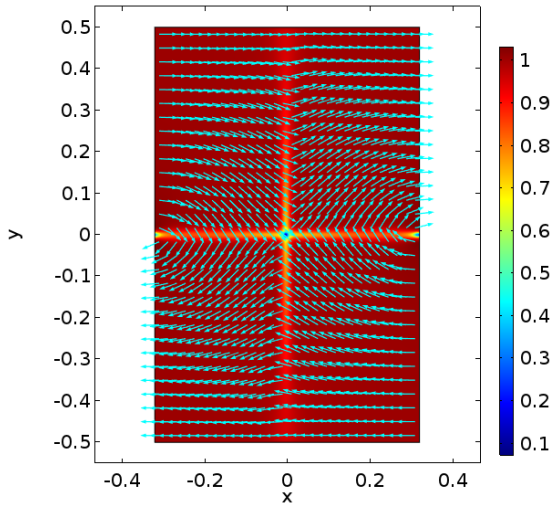

FIG. 6.1. *A solution u of the Euler–Lagrange equation associated with the energy functional (1.1) in the rectangle $[-T,T]\times[-1/2,1/2]$ subject to periodic boundary conditions on $\{-T,T\}\times[-1/2,1/2]$ and assuming that $u(\cdot,\pm1/2)=(\pm1,0)$. Here $L=1/2$ and $T=\tilde{T}(1)/2\approx 0.3$. Both u and $|u|$ are shown.*

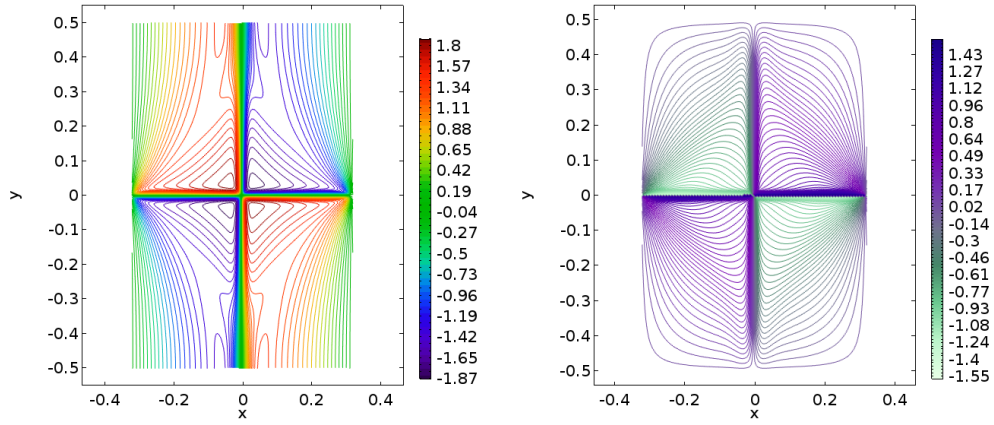

FIG. 6.2. *Level curves for the divergence of u (left) and the angle θ (right), where $u=(\cos\theta,\sin\theta)$ is depicted in Figure* 6.1.

In our numerics, we fixed $H=1/2$ and allowed L to vary. Then, for a given $L>0$, we determined $T=\tilde{T}(2L)/2$ by solving (6.30). The reason for this choice of T will be explained below. The Euler–Lagrange equation for E_ε was then solved on the rectangle $(-T,T)\times(-1/2,1/2)$, subject to periodic boundary conditions on $\{-T,T\}\times[-1/2,1/2]$ and assuming that $u(\cdot,\pm1/2)=(\pm1,0)$.

Our numerical studies allowed us to identify three different regimes. When L is small, the one-dimensional solution (not shown) is recovered as the result of simulations. For intermediate values of L, a single-wall cross-tie configuration appears (Figures 6.1–6.2). An analytical solution corresponding to this configuration will be constructed below using the conservation laws approach of Corollary 4.2. To this end, we observe that (i) this configuration has both vertical and horizontal jump sets coin-

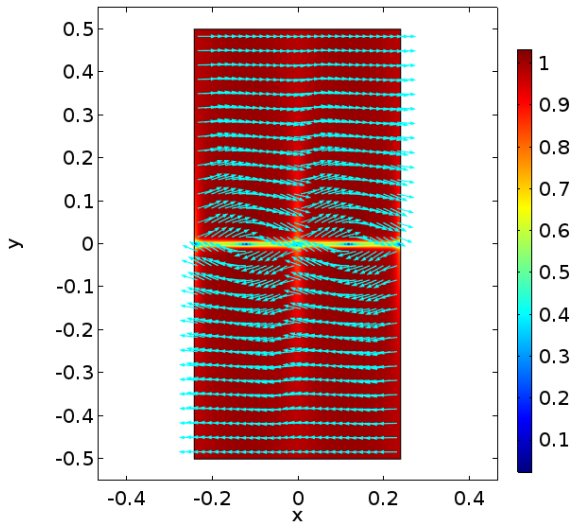

FIG. 6.3. *A solution u of the Euler–Lagrange equation associated with the energy functional (1.1) in the rectangle $[-T,T]\times[-1/2,1/2]$ subject to periodic boundary conditions on $\{-T,T\}\times[-1/2,1/2]$ and assuming that $u(\cdot,\pm 1/2)=(\pm 1,0)$. Here $L=3/2$ and $T=\tilde{T}(3)/2\approx 0.25$. Both u and $|u|$ are shown.*

ciding with the coordinate axes as well as a pair of defects of degrees ± 1 at $(0,T)$ and $(0,0)$, respectively; (ii) the solution is symmetric with respect to reflections about the coordinate axes, and the divergence is antisymmetric with respect to these reflections; and (iii) the level curves for divergence in the first quadrant can be categorized into three different regions, as in Figure 6.5.

We conjecture that this configuration corresponds to the cross-tie construction that we develop in this section. Indeed, when the solution resulting from this construction is plotted (Figure 6.6), it closely resembles those in Figure 6.2.

Before proceeding with the analytical construction of a cross-tie configuration resembling Figure 6.1, we continue with further remarks about our E_ε numerics for larger values of L. When L is increased further, it appears that $2T=\tilde{T}(2L)$, as determined by (6.30), is no longer the period of the optimal construction, as two cross-tie structures appear on the interval $[-T,T]$ in Figures 6.3–6.4. We call this a type-II cross-tie configuration. A close examination of Figure 6.3 shows that the level curves for divergence that originate on the y-axis appear to terminate on the line $y=1/2$, as opposed to those in Figures 6.1–6.2. Pursuing an analytical construction of this solution is beyond the scope of the present paper. However, it follows that we can identify at least three families of critical points that may minimize the limiting energy functional E_0 for different values of L.

Analytical construction of a cross-tie configuration and the proof of Theorem 6.6. We now use the observations made concerning the numerics of a single cross-tie to construct a critical point of E_0. Although numerics were carried out fixing $H=1/2$, we will carry out our construction for any H and work on a single period cell $\Omega=(0,2T)\times(-H,H)$. We will further assume $T<H$, a choice that is consistent with the choice made in the numerics.

A single period cell of this solution is composed of a dipole, i.e., a pair of $+1$ and -1 vortices, along with walls connecting them. The above observations (i)–(iii) from

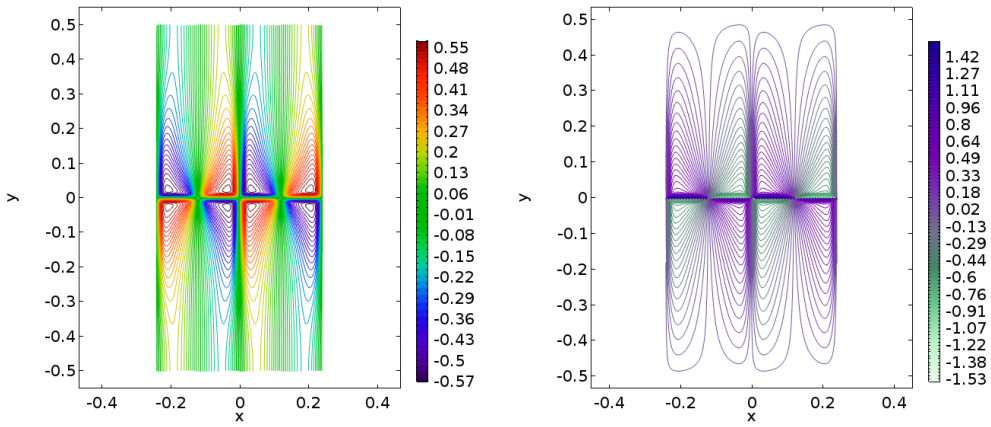

FIG. 6.4. *Level curves for the divergence of u (left) and the angle θ (right), where $u = (\cos\theta, \sin\theta)$ is a type-II cross-tie depicted in Figure* 6.3.

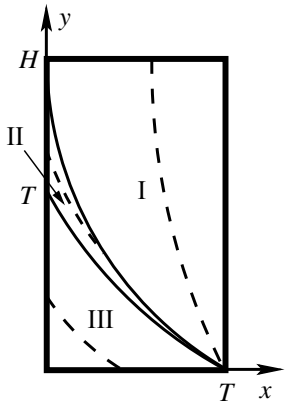

FIG. 6.5. *Regions corresponding to different characteristics families. Typical characteristics for each region are indicated by dashed lines.*

the numerics motivate us to construct the critical point $u = (\cos\theta, \sin\theta)$ on a quarter of the period cell, say $\omega := (0, T) \times (0, H)$, and define u elsewhere by appropriate reflections. A quarter period cell is displayed in Figure 6.5. By comparison with Figure 6.1, the line $x = 0$, $0 \leqslant y \leqslant H$ denotes a vertical wall, and the x-axis denotes a horizontal wall. Upon reflection and periodic extension, the point $(0, 0)$ is to house a degree -1 vortex, while at the point $(T, 0)$ we will have constructed a $+1$ vortex resembling the $\widehat{e}_\theta$ vector.

We construct solutions to the system of conservation laws given in Corollary 4.2 using the method of characteristics. Within the quarter period cell ω under consideration, we seek $u = (\cos\theta, \sin\theta)$ with $\theta \in [0, \frac{\pi}{2}]$. We impose Dirichlet boundary conditions $\theta = 0$ along the top and right boundaries of ω. The condition on the right boundary is a result of the symmetry observation (ii) above. The natural boundary condition (4.2) is to be satisfied along the left boundary and the x-axis since these represent walls.

Building on observation (iii), the characteristics solution in ω consists of three families of circular arcs, labeled regions I through III in Figure 6.5 and described

in Steps 1–3 below. In each of the regions I, II, and III above, we will denote the arc-length and characteristic variables by s_1, s_2, s_3 and t_1, t_2, t_3, respectively. The dependent variables $x = x(s,t)$, $y = y(s,t)$, $\theta = \theta(s,t)$, and $v = v(s,t)$ will also be denoted using appropriate subscripts.

Step 1. In this step, we construct characteristics foliating region I in Figure 6.5. First, starting from the top boundary $\{(s_1, H) : 0 \leqslant s_1 \leqslant T\}$, we issue characteristics that meet at the point $(T, 0)$. Indeed, along the top boundary, we have the boundary condition $\theta_1 = 0$, since $a = 0$. By the characteristic equations, characteristics emanating from (s_1, H) for any $0 \leqslant s_1 \leqslant T$ leave the top boundary orthogonally. For such fixed s_1, there is a unique circle orthogonal to the top boundary at (s_1, H) that passes through the point $(T, 0)$. A geometric argument shows that the center of this circle is given by $\left(\frac{T+s_1}{2} + \frac{H^2}{2(T-s_1)}, H\right)$, while the radius is given by

$$R(s_1) = \frac{T - s_1}{2} + \frac{H^2}{2(T - s_1)}. \tag{6.22}$$

It follows that $R(s_1) \geqslant H$. Integrating the characteristics starting at the top boundary, the circles constructed are characteristics, and along the circle starting at (s_1, H), we have $v_1(s_1, t_1) \equiv v_1(s_1) := \frac{1}{R(s_1)}$ and $\theta_1(s_1, t_1) = v_1(s_1)t_1$.

It is clear that the foregoing yields characteristics that only meet at $(T, 0)$ and not before. Furthermore, the right boundary of ω, along which $\theta_1 = 0$, is itself a characteristic and belongs to the above family corresponding to infinite radius, as can be observed by setting $s_1 = T$ in (6.22). Furthermore, it is clear that the divergence is bounded for this family, i.e., $v_1(s_1) \in [0, H]$.

The characteristic emanating out of $(0, H)$ satisfies $v_1(0) = \frac{1}{R(0)} = \frac{2T}{T^2+H^2} =: \alpha$. For later use, we record the equation of this characteristic as being given by

$$x_1(t_1) = -\frac{1}{\alpha}\left(\cos\left(\alpha t_1\right) - 1\right), \qquad y_1(t_1) = H - \frac{1}{\alpha}\sin\left(\alpha t_1\right). \tag{6.23}$$

We will refer to this characteristic as the terminal characteristic of the first family and denote it by Γ. If we let t_1^* denote the time of arrival of this characteristic at $(T, 0)$, then we have the relation

$$\frac{H}{\sin\left(\alpha t_1^*\right)} = \frac{T}{1 - \cos\left(\alpha t_1^*\right)}, \tag{6.24}$$

which we can also write as

$$\tan\left(\frac{\alpha t_1^*}{2}\right) = \frac{T}{H}. \tag{6.25}$$

Step 2. In this step, we construct a family of characteristics that foliate region III of Figure 6.5. This family of characteristics consists of circular arcs emanating from $(s_3, 0)$ and terminating on the vertical wall at $(0, y_3(t_3^*(s_3)))$ for $s_3 \in (0, T)$. The symmetry assumptions from observations (ii)–(iii) along with (4.2) yield $Lv_3 + \sin 2\theta_3 = 0$ along both the left and bottom walls. Since the divergence v_3 is constant along characteristics, we find that $\sin 2\theta_3(s_3, 0) = \sin 2\theta_3(s_3, t_3^*(s_3))$, yielding

$$\theta_3(s_3, t_3^*(s_3)) = \frac{\pi}{2} - \theta_3(s_3, 0). \tag{6.26}$$

Writing down the condition that $(x_3(s_3, t_3^*(s_3)), y_3(s_3, t_3^*(s_3)))$ lies on the left wall, i.e. $x_3(s_3, t_3^*(s_3)) = 0$, along with (4.2) along this wall, yields upon some elementary computations that

$$\sin 2\theta_3(s_3, 0) = \frac{-1 + (1 + 2\lambda)^{1/2}}{\lambda}, \qquad \lambda = \frac{2s_3^2}{L^2}. \tag{6.27}$$

It can be checked that the right-hand side of the last equation defining $\sin 2\theta_3(s_3, 0)$ indeed belongs to the interval $(0, 1)$. Integrating the characteristic equations, we find that the circular arcs of the family foliating region III are characteristics along which we have $v_3(s_3, t_3) := v_3(s_3) = -\frac{\sin 2\theta_3(s_3,0)}{L}$. It can also be easily checked that the particular characteristic of this family originating at $(T, 0)$ satisfies

$$y_3(T, t_3^*(T)) = T. \tag{6.28}$$

We will refer to this characteristic as the terminal characteristic of the family foliating region III.

For reasons that will be clear in the next step, we require that the terminal characteristic of the families foliating regions I and III, respectively, are tangent at $(T, 0)$. This condition can be rewritten, using (6.24) and (6.27), as

$$\frac{L^2}{T^2}\left(\sqrt{1 + 4\frac{T^2}{L^2}} - 1\right) = \frac{8TH}{T^2 + H^2}\frac{H^2 - T^2}{H^2 + T^2}. \tag{6.29}$$

Before continuing, we remark about relation (6.29). The left-hand side is a function of L/T, while the right-hand side is a function of H/T alone, which we are assuming to be greater than one. We claim that for any $x := H/T > 1$, there exists a unique L/T such that (6.29) holds. Indeed, setting $\zeta = \frac{2x}{x^2+1}\frac{x^2-1}{x^2+1} < 1$ and $\Lambda = \frac{4T^2}{L^2}$, we are required to solve

$$\sqrt{1 + \Lambda} = 1 + \zeta\Lambda.$$

We obtain that $\Lambda = \frac{1-2\zeta}{\zeta^2}$, which is positive, provided $\zeta < 1/2$, or equivalently, provided $2x(x^2 - 1) < \frac{1}{2}(x^2 + 1)^2$. This is clear since

$$\frac{1}{2}(x^2 + 1)^2 - 2x(x^2 - 1) = \left(\frac{1}{\sqrt{2}}(x^2 - 1) - \sqrt{2}x\right)^2.$$

Introducing the rescaling $\tilde{T} = T/H$, we denote by $\tilde{T}(L/H)$ the unique solution of

$$L/H\left(\sqrt{(L/H)^2 + 4\tilde{T}^2} - L/H\right) - \frac{8\tilde{T}^3\left(1 - \tilde{T}^2\right)}{\left(\tilde{T}^2 + 1\right)^2} = 0 \tag{6.30}$$

for a given value of L/H. In what follows, we set $T = H\tilde{T}(L/H)$.

We conclude this part with the following observation. Equation (6.25) can now be written as

$$\tilde{T} = \tan\left(\frac{\alpha t_1^*}{2}\right),$$

and testing (6.30) with $\alpha t_1^* = \frac{\pi}{4}$ and $\alpha t_1^* = \frac{\pi}{2}$, we observe that the left-hand side is negative and positive, respectively. By the intermediate value theorem, it then follows that $\alpha t_1^* \in \left[\frac{\pi}{4}, \frac{\pi}{2}\right]$ for all $L > 0$. With the help of (6.26) we can now conclude that

$$\theta_3(T, t_3^*(T)) \in \left[0, \frac{\pi}{4}\right]. \tag{6.31}$$

Step 3. We finally foliate region II by characteristics to define our critical point in this region. Since $H > T$ by assumption, it remains to fill the gap between the circles of the first two families. In brief, we issue secondary characteristics that emanate from the $s = 0$ characteristic Γ of the first family tangentially, to meet the left wall. The divergence v has a jump discontinuity along Γ, while the tangential departure of the secondary characteristics from Γ renders θ continuous across Γ.

In more detail, we write the initial curve Γ using s as the arc-length parameter (cf. Step 1) to get

$$x_0(s_2) = \frac{1}{\alpha}\big(1 - \cos(\alpha s_2)\big), \qquad y_0(s_2) = H - \frac{1}{\alpha}\sin(\alpha s_2),$$

and the initial condition on θ is given by $\theta_0(s_2) = \alpha s_,$ where $s_2 \in [0, t_1^*]$ and t_1^* is as in (6.24). We do not set an initial condition on the divergence v_2, but instead determine v_2 by enforcing (4.2) at the left wall. Integrating the characteristic equations, we find

$$v_2(s_2, t_2) = v_2(s_2), \quad \theta_2(s_2, t_2) = \theta_0(s_2) + v_2(s_2)t_2, \tag{6.32}$$

$$\begin{aligned} x_2(s_2, t_2) &= \frac{1}{\alpha}\big(1 - \cos(\alpha s_2)\big) + \frac{1}{v_2(s_2)}\left(\cos\theta_2(s_2, t_2) - \cos\alpha s_2)\right), \\ y_2(s_2, t_2) &= H - \frac{1}{\alpha}\sin(\alpha s_2) + \frac{1}{v_2(s_2)}\left(\sin\theta_2(s_2, t_2) - \sin\alpha s_2\right). \end{aligned} \tag{6.33}$$

Again, defining $t_2^*(s_2)$ to be the time of arrival of the characteristic originating at $(x_0(s_2), y_0(s_2))$ to the y-axis, we obtain, using (6.32), (6.33), and (4.2) and denoting $\theta_2^*(s_2) := \theta_2(s_2, t_2^*(s_2))$,

$$\begin{aligned} \frac{1}{\alpha}\big(1 - \cos(\alpha s_2)\big) + \frac{1}{v_2(s_2)}\left(\cos\theta_2^*(s_2) - \cos\alpha s_2\right) = 0, \\ L v_2(s_2) + \sin 2\theta_2^*(s_2) = 0. \end{aligned} \tag{6.34}$$

If we define a function $f = f(\beta, s_2)$ via the formula

$$f(\beta, s_2) := (1 - \cos(\alpha s_2))\sin 2\beta - L\alpha(\cos\beta - \cos(\alpha s_2)), \tag{6.35}$$

then substituting the second of the equations in (6.34) into the first, we find that θ_2^* must satisfy the condition $f(\theta_2^*(s_2), s_2) = 0$. We note that $f(0, s_2) < 0$ for any $s_2 > 0$. Now with an eye towards applying the intermediate value theorem, we define $\beta^* = \beta^*(s_2)$ via

$$\sin\beta^* = \begin{cases} \frac{L\alpha}{2\left(1-\cos(\alpha s_2)\right)} & \text{if } L\alpha \leqslant 2\big(1 - \cos(\alpha s_2)\big), \\ 1 & \text{otherwise.} \end{cases}$$

One easily checks that $f(\beta^*(s_2), s_2) > 0$ for $s_2 > 0$. Hence, the desired terminal angle $\theta_2^*(s_2)$ exists for all s_2.

Furthermore, differentiating (6.35), and setting $\beta = \theta_2^*(s_2)$, with respect to s_2, we find that

$$\frac{d\theta_2^*}{ds_2} = \frac{(L\alpha - \sin 2\theta_2^*)\alpha \sin(\alpha s_2)}{2(1-\cos(\alpha s_2))\cos 2\theta_2^* + L\alpha \sin\theta_2^*}.$$

Our goal is to show that $\frac{d\theta_2^*}{ds_2} > 0$. We start first by showing that the denominator of the fraction defining this derivative is positive. For each fixed s_2, the function D prescribed by

$$D(\sin\beta, s_2) := 2(1-\cos(\alpha s_2))(1-2\sin^2\beta) + L\alpha \sin\beta$$

defines a downward-facing quadratic in $\sin\beta$. We note that $D(0, s_2) = 2(1-\cos(\alpha s_2)) > 0$, and an easy calculation shows that $D(\sin\beta^*, s_2) > 0$. It follows easily that $D(\sin\theta^*(s_2), s_2) > 0$, which is precisely the denominator of the fraction defining $\frac{d\theta_2^*}{ds_2}$.

We must show that the numerator of this fraction is also positive. This is immediate when $L\alpha \geqslant 1$, and therefore we must provide an argument for when $L\alpha < 1$. Define the number $\beta_- \in [0, \pi/4]$ using the formula $\sin 2\beta_- = L\alpha$. Then note that $f(\beta_-, s_2) > 0$. Therefore, when $L\alpha \leqslant 1$, we have that in fact $\theta_2^*(s_2) < \min(\beta_-, \beta^*) \leqslant \pi/4$. Consequently, for such $L\alpha$ values, we have that $L\alpha - \sin 2\theta_2^* > L\alpha - \sin 2\beta_- = 0$.

This completes the proof of the claim that θ^* is increasing as a function of s. Combining this fact with the constraint (6.31), we have

$$\theta_2^*(T) = \theta_3(T, t_3^*(T)) \in \left[0, \frac{\pi}{4}\right],$$

and hence

$$\theta_2^*(s_2) \in \left[0, \frac{\pi}{4}\right] \text{ for all } s_2 \in [0, T].$$

Equation (6.34) can now be used to show that v_2 is both negative and decreasing. The proof that the characteristics foliate region II then proceeds exactly as in Lemma 5.1, completing the construction of our cross-tie critical point.

Having completed the construction of the critical point u of E_0 on all of Ω by appropriate reflections, towards proving Theorem 6.6, it remains to compute $E_0(u)$ and compare it with that of the one-dimensional minimizer from Theorem 6.4. The energies per period for the different competitors are compared in Figure 6.7. Recall that, by Remark 6.7, the energy density per period is a function of the scaled elastic constant L/H. The solid and dashed lines in Figure 6.7 represent the energies of the one-dimensional and the two-dimensional characteristics cross-tie constructions, respectively. Here the energy of a one-dimensional competitor is given in the statement of Theorem 6.4, and the energy of the two-dimensional construction is obtained by computing an appropriate Jacobian and numerically integrating in MATLAB [2] (or by using the coarea formula). Comparing these energies for $L/H \in (L_0, L_1)$, Theorem 6.6 now follows.

Further numerical observations are in order. When the solution resulting from the characteristics construction is plotted (Figure 6.6), it closely resembles those in Figure 6.2. The markers in Figure 6.7 represent the energies of the numerically computed solutions to the Euler–Lagrange equations for E_ε, where the shape of the marker distinguishes the type of the energy-minimizing solution obtained in the simulations. We can observe a close correspondence between the numerics and analytical solutions as the squares and circles track well the one- and two-dimensional constructions, respectively. While the two-dimensional cross-tie construction discussed above has

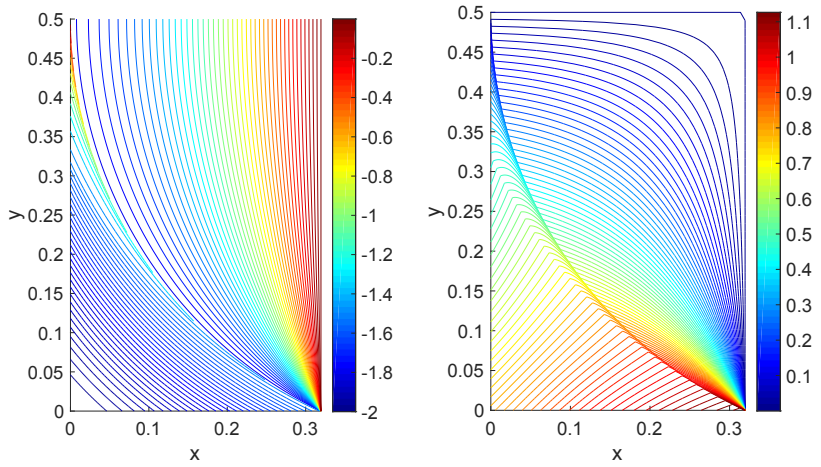

FIG. 6.6. *Level curves for the divergence of u (left) and the angle θ (right), where $u = (\cos\theta, \sin\theta)$ is a solution obtained using characteristics. Here $L = 1$.*

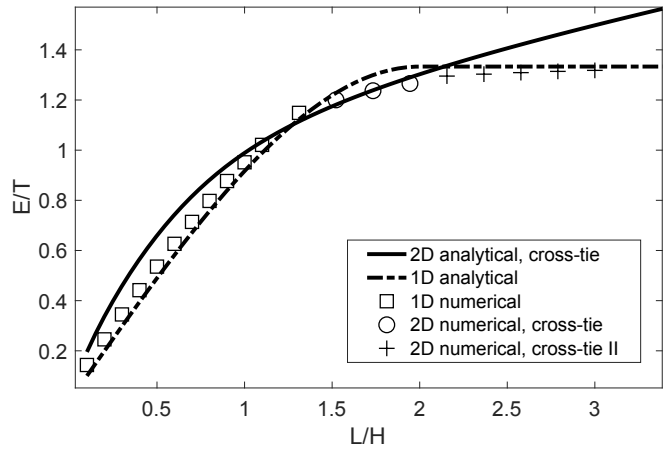

FIG. 6.7. *Energy per unit length.*

a smaller energy (both theoretically and numerically) on a short interval of L values, it is then superseded by the two-dimensional cross-tie type-II configurations of Figures 6.3–6.4. Indeed, this configuration still has a smaller energy than the one-dimensional construction. The difference between the energies of the one-dimensional and the two-dimensional cross-tie type-II constructions is small, however, and appears to decrease with an increasing L.

We conclude with a few conjectures suggested by numerics.

Conjecture 1. For $0 < L/H < L_0$, the one-dimensional minimizer from Theorem 6.4 is a unique minimizer of E_0 among all two-dimensional competitors.

Conjecture 2. For $L/H \in (L_0, L_1)$, the critical point constructed in the proof of Theorem 6.6 is a minimizer of E_0.

Conjecture 3. For $L/H \geqslant L_1$, there exists a two-dimensional minimizer u_L with $E_0[u_L]$ that is lower than the minimum energy achieved over one-dimensional com-

petitors. The difference in energies, however, vanishes in the $L \to \infty$ limit. Moreover, the unique cluster point of u_L in $H_{\mathrm{div}}(\Omega;\mathbb{S}^1) \cap BV(\Omega;\mathbb{S}^1)$ is given by the piecewise constant vector field, which equals $(1,0)$ for $y > 0$ and equals $(-1,0)$ for $y < 0$.

REFERENCES

[1] *COMSOL Multiphysics*, v. 5.3 COMSOL AB, Stockholm, Sweden, http://www.comsol.com/.

[2] *MATLAB* 9.3, Release R2017b, The MathWorks, Inc., Natick, MA, 2017.

[3] F. Alouges, T. Rivière, and S. Serfaty, *Néel and cross-tie wall energies for planar micromagnetic configurations*, ESAIM Control Optim. Calc. Var., 8 (2002), pp. 31–68, https://doi.org/10.1051/cocv:2002017.

[4] L. Ambrosio, C. De Lellis, and C. Mantegazza, *Line energies for gradient vector fields in the plane*, Calc. Var. Partial Differential Equations, 9 (1999), pp. 327–255, https://doi.org/10.1007/s005260050144.

[5] P. Aviles and Y. Giga, *On lower semicontinuity of a defect energy obtained by a singular limit of the Ginzburg-Landau type energy for gradient fields*, Proc. Roy. Soc. Edinburgh Sect. A, 129 (1999), pp. 1–17, https://doi.org/10.1017/S0308210500027438.

[6] A. C. Barroso and I. Fonseca, *Anisotropic singular perturbations—the vectorial case*, Proc. Roy. Soc. Edinburgh Sect. A, 124 (1994), pp. 527–571, https://doi.org/10.1017/S0308210500028778.

[7] F. Bethuel, H. Brezis, and F. Hélein, *Ginzburg-Landau Vortices*, Progr. Nonlinear Differential Equations Appl. 13, Birkhäuser Boston, Boston, MA, 1994, https://doi.org/10.1007/978-1-4612-0287-5.

[8] S. Conti and C. De Lellis, *Sharp upper bounds for a variational problem with singular perturbation*, Math. Ann., 338 (2007), pp. 119–146, https://doi.org/10.1007/s00208-006-0070-2.

[9] C. De Lellis and F. Otto, *Structure of entropy solutions to the eikonal equation*, J. Eur. Math. Soc. (JEMS), 5 (2003), pp. 107–145, https://doi-org.proxyiub.uits.iu.edu/10.1007/s10097-002-0048-7.

[10] A. DeBenedictis and T. J. Atherton, *Shape minimisation problems in liquid crystals*, Liquid Crystals, 43 (2016), pp. 2352–2362, https://doi.org/10.1080/02678292.2016.1209699.

[11] A. Desimone, R. V. Kohn, S. Müller, and F. Otto, *Repulsive interaction of Néel walls, and the internal length scale of the cross-tie wall*, Multiscale Model. Simul., 1 (2003), pp. 57–104, https://doi.org/10.1137/S1540345902402734.

[12] A. DeSimone, S. Müller, R. V. Kohn, and F. Otto, *A compactness result in the gradient theory of phase transitions*, Proc. Roy. Soc. Edinburgh Sect. A, 131 (2001), pp. 833–844, https://doi.org/10.1017/S030821050000113X.

[13] J. L. Ericksen, *Liquid crystals with variable degree of orientation*, Arch. Rational Mech. Anal., 113 (1990), pp. 97–120, https://doi.org/10.1007/BF00380413.

[14] D. Golovaty, *On a Γ-limit of a family of anisotropic singular perturbations*, Manuscripta Math., 92 (1997), pp. 515–524, https://doi.org/10.1007/BF02678209.

[15] D. Golovaty, P. Sternberg, and R. Venkatraman, *A Ginzburg-Landau Type Problem for Highly Anisotropic Nematic Liquid Crystals*, preprint, https://arxiv.org/abs/1712.00493, 2017.

[16] F. Hélein, *Minima de la fonctionnelle énergie libre des cristaux liquides*, C.R. Acad. Sci. Paris Sér. I Math., 305 (1987), pp. 565–568.

[17] R. Ignat, *Singularities of divergence-free vector fields with values into S^1 or S^2. Applications to micromagnetics*, Confluentes Math., 4 (2012), 1230001, https://doi.org/10.1142/S1793744212300012.

[18] P.-E. Jabin, F. Otto, and B. Perthame, *Line-energy Ginzburg-Landau models: Zero-energy states*, Ann. Sc. Norm. Super. Pisa Cl. Sci. (5), 1 (2002), pp. 187–202.

[19] W. Jin and R. V. Kohn, *Singular perturbation and the energy of folds*, J. Nonlinear Sci., 10 (2000), pp. 355–390, https://doi.org/10.1007/s003329910014.

[20] R. V. Kohn, *Energy-driven pattern formation*, in International Congress of Mathematicians. Vol. I, Eur. Math. Soc., Zürich, 2007, pp. 359–383, https://doi.org/10.4171/022-1/15.

[21] X. Lamy and F. Otto, *On the regularity of weak solutions to Burgers equation with finite entropy production*, Calc. Var. Partial Differential Equations, 57 (2018), p. 94.

[22] A. Lorent, *A quantitative characterisation of functions of low Aviles Giga energy in convex domains*, Ann. Sc. Norm. Super. Pisa Cl. Sci. (5), 13 (2014), pp. 1–66.

[23] N. J. Mottram and C. J. Newton, *Introduction to Q-Tensor Theory*, preprint, https://arxiv.org/abs/1409.3542, 2014.

[24] T. Rivière and S. Serfaty, *Compactness, kinetic formulation, and entropies for a problem*

related to micromagnetics, Comm. Partial Differential Equations, 28 (2003), pp. 249–269, https://doi.org/10.1081/PDE-120019381.

[25] R. Temam, *Navier-Stokes Equations. Theory and Numerical Analysis*, Stud. Math. Appl. 2, North-Holland, Amsterdam, New York, Oxford, 1977,

[26] E. G. Virga, *Variational Theories for Liquid Crystals*, Appl. Math. Math. Comput. 8, Chapman & Hall, London, 1994, https://doi.org/10.1007/978-1-4899-2867-2.

[27] S. Zhou, Y. A. Nastishin, M. M. Omelchenko, L. Tortora, V. G. Nazarenko, O. P. Boiko, T. Ostapenko, T. Hu, C. C. Almasan, S. N. Sprunt, J. T. Gleeson, and O. D. Lavrentovich, *Elasticity of lyotropic chromonic liquid crystals probed by director reorientation in a magnetic field*, Phys. Rev. Lett., 109 (2012), 037801, https://doi.org/10.1103/PhysRevLett.109.037801.